AN EXPERIMENTAL INVESTIGATION OF HEAT TRANSFER FROM AN ISOTHERMAL CYLINDER EXPOSED TO TWO-COMPONENT CROSSFLOW

A THESIS

Presented to

The Faculty of the Graduate Division

by

Robert Theodore Saterbak

In Partial Fulfillment

of the Requirements for the Degree

Master of Science in Mechanical Engineering

Georgia Institute of Technology

June, 1967

AN EXPERIMENTAL INVESTIGATION OF HEAT TRANSFER FROM AN ISOTHERMAL CYLINDER EXPOSED TO TWO-COMPONENT CROSSFLOW

Approved:

Chairman

Date approved by Chairman: May 25, 1967

In presenting the dissertation as a partial fulfillment of the requirements for an advanced degree from the Georgia Institute of Technology, I agree that the Library of the Institute shall make it available for inspection and circulation in accordance with its regulations governing materials of this type. I agree that permission to copy from, or to publish from, this dissertation may be granted by the professor under whose direction it was written, or, in his absence, by the Dean of the Graduate Division when such copying or publication is solely for scholarly purposes and does not involve potential financial gain. It is understood that any copying from, or publication of, this dissertation which involves potential financial gain will not be allowed without written permission.

3/17/65
b

ACKNOWLEDGMENTS

The author would like to express his sincere appreciation to all those who made this work possible. In particular, he would like to thank Dr. J. E. Sunderland, his advisor, whose instruction and advice were invaluable throughout this work. Further, he would like to thank Dr. C. W. Gorton and Dr. N. R. Johnson for their advice and service on the reading committee, and Dr. T. W. Jackson who helped initiate this research project. Also, a special note of thanks is extended to his co-workers, Messrs. J. W. Hodgson, W. C. Thomas, and R. S. Rudland, with whom is shared the credit of fabrication of the experimental apparatus.

The author would like to express his gratitude for the National Science Foundation Grant No. GK-766 which provided funds for equipment making this research possible and for partial support for his graduate study.

Finally, the author would like to express his sincere appreciation to his wife, Celia Ann, and his father, Mr. W. Saterbak, without whose love, encouragement, and help this work would not have been possible.

TABLE OF CONTENTS

TABLE OF CONTENTS (Continued)

LIST OF TABLES

LIST OF TABLES (Continued)

LIST OF ILLUSTRATIONS

LIST OF ILLUSTRATIONS (Continued)

SUMMARY

An experimental and analytical study of the heat transfer characteristics of an isothermal circular cylinder exposed to a saturated air stream with entrained water droplets was undertaken. The effects of the air free stream Reynolds number and the water-air mass flow rate ratio on the local and overall Nusselt numbers were studied. This study included only the situation where sensible heating of the liquid film was significant.

A two-component (air-water) flow closed loop wind tunnel, a water spray system, an internally heated cylinder, and temperature and power measuring equipment were designed, constructed, assembled, and calibrated. A vertical test section area was provided with a three-inch diameter brass test cylinder mounted horizontally.

The integral forms of the continuity, momentum, and energy equations were developed and solved for a simplified analytical model of the liquid film on the upstream side of the cylinder. It was assumed that the gas and liquid droplets had the same temperature and velocity upstream of the cylinder. It was also assumed that the liquid droplets were captured by the liquid film with no "splashing" and formed a laminar boundary layer. Linear velocity and temperature profiles were assumed for the liquid boundary layer. Only sensible heating of the liquid film was considered significant while convective and evaporative heat transfer of the liquid film were considered negligible.

Experimental tests were performed for air free stream Reynolds

numbers of 30,000, 75,000, and 118,000, and water-air mass flow rate ratios varying from 0.012 to 0.13. The analytical results agreed favorably with the experimental results. Both the experimental and analytical results showed that the addition of water droplets to the air stream greatly increased the heat transfer from the cylinder over that which would have been obtained from a one-component (air) crossflow.

NOMENCLATURE

English Letters		Typical Units
a	non-dimensional coefficient (p.44)	dimensionless
A	area	ft^2
b	non-dimensional coefficient (p.44)	dimensionless
c	dimensional coefficient (p.48)	^oF
c_p	specific heat	BTU/lbm ^oF
d	dimensional coefficient (p.48)	^oF
D	diameter of cylinder	ft
$\bar{e}_p$	probe efficiency (p.30)	dimensionless
g_c	gravitational conversion factor	lbm ft/lbf-sec^2
h	heat transfer coefficient	BTU/hr ft^2 ^oF
H	enthalpy	BTU/lbm
k	thermal conductivity	BTU/hr ft ^oF
$\dot{m}$	mass flow rate	lbm/ft^2-sec
$\bar{m}$	non-dimensional mass flow rate (p.49)	dimensionless
N	average water droplet collection rate	cc/sec
Nu	Nusselt number (pp. 7 and 51)	dimensionless
P	pressure	lbf/ft^2
Pr	Prandtl number	dimensionless
Q	cartridge heater power output	BTU/hr
r	radius	ft
$\bar{r}$	non-dimensional radius (p.44)	dimensionless

English Letters		Typical Units
R	radius of cylinder	ft
Re	Reynolds number	dimensionless
T	temperature	^{o}F
U	liquid film velocity in θ-direction	ft/sec
U_{∞}	liquid droplet velocity upstream of the cylinder	ft/sec

Greek Letters		
δ	thickness of liquid film	ft
$\bar{\delta}$	non-dimensional liquid film thickness (p.45)	dimensionless
θ	angular co-ordinate measured from stagnation point	degrees
μ	absolute viscosity	lbm/ft-sec
ν	kinematic viscosity	ft^2/sec
$\bar{\nu}$	non-dimensional kinematic viscosity (p.51)	dimensionless
ρ	density	lbm/ft^3
$\bar{\rho}$	non-dimensional density (p.49)	dimensionless
τ	shear stress	lbf/ft^2
ϕ	non-dimensional temperature (p.48)	dimensionless
Ψ	temperature parameter (p.48)	^{o}F

Subscripts

a	air
D	cylinder diameter
g	gas

Subscripts

l	liquid
s	local value at cylinder surface
w	water
δ	values at gas-liquid interface
θ	values at angular co-ordinate measured from the stagnation point
∞	values upstream of the cylinder

CHAPTER I

INTRODUCTION

General Introduction

In recent years, an increasing emphasis has been placed on methods to increase the heat transfer from a body to a cooling medium. Several directions have been pursued, including ablation cooling, transpiration cooling, and film cooling. In film cooling, ejection of a gas or a liquid through slots in the walls of the body is the usual method. Another method of film cooling is to spray liquid droplets into a gas stream flowing past the body. Under certain conditions, a continuous liquid film is formed on the body and the heat transfer from the externally wetted surface of the body is greatly increased over that obtained from only a gas stream. In particular, the problem of external heat transfer from an isothermal cylinder exposed to a two-component mixture, consisting of water droplets borne by a saturated air stream, is studied.

Survey of Previous Investigations

At present, only a limited number of references concerning the study of heat transfer from a cylinder exposed to a two-component crossflow have been published.

An analytical and experimental study of a heated, vertical cylinder exposed to a two-component (air-water) crossflow was recently presented by Acrivos, et al. (1). Four different analytical models of droplet behavior upon contact with the cylinder surface were presented. In the first

model, the liquid droplets impinging on the heated cylinder were assumed to vaporize instantly upon contact with the cylinder. In the next two models, a liquid film was assumed to form on the cylinder. In one case, the liquid was assumed to evaporate from the cylinder; in the other case, the liquid absorbed energy from the cylinder as sensible heat with no evaporation. In the fourth model, the liquid droplets bounced off the cylinder after impingement. The experimental analysis indicated that only under extreme situations did conditions corresponding to the first model exist. Under ordinary conditions, a liquid film covered the cylinder surface. The fourth model was not evaluated due to its complexity. Therefore, most of the data corresponded to the second and third models. Experimental tests were reported at air free stream Reynolds numbers of 43,000 and 80,000 and water mass flow rates of 0.014 and 0.083 lbm/sec. The overall heat transfer coefficients in two-component flow were from 2.5 to 9.0 times greater than in one-component (air) flow. A non-uniform water spray distribution onto the test cylinder resulted in non-symmetric heat transfer around the cylinder. Spray water splashing and dripping was reported on the downstream side of the cylinder. In determining the heat transfer coefficient, the temperature difference between the cylinder surface and the water droplets before they were sprayed into the air stream was used.

A report by Hoelscher (2) has been presented, basically verifying the report by Acrivos. This report was an experimental investigation to determine the effects of the water-air mass flow rate ratio on the local and overall heat transfer coefficients for a given air free stream Reynolds number. An air free stream Reynolds number of 118,000 and water-air

mass flow rate ratios varying from 0.016 to 0.053 were considered. The report indicated that heat transfer occurred almost entirely on the upstream side of the cylinder, with an increase in the overall heat transfer coefficient as the water-air mass flow rate ratio increased. The investigation reported a negative heat transfer coefficient on the downstream side of the cylinder, apparently caused by heat conduction from the upstream side of the cylinder through the insulated sections. Hoelscher referenced the temperature difference between the cylinder surface and the air temperature before water was injected into the air stream.

An extension of Hoelscher's experimental work was reported by Takahara (3). The effects of the water-air mass flow rate ratio and the air free stream Reynolds number on the local and overall heat transfer coefficients around a vertical cylinder in two-component (air-water) flow were studied. Takahara reported data at air free stream Reynolds numbers of 48,000, 77,000, and 110,000 with water-air mass flow rate ratios varying from 0.028 to 0.058. It was found that the overall heat transfer coefficient increased as the water-air mass flow rate ratio increased. Likewise, as the Reynolds number increased, the overall heat transfer coefficient increased. Takahara reported identical air and water droplet temperatures and used this temperature and the cylinder surface temperature as the temperature difference in determining the film heat transfer coefficients.

Smith (4) recently presented an analytical and experimental study of a heated, horizontal cylinder exposed to a two-component (air-water) flow. An analytical study of the heat transfer characteristics on the upstream side of the cylinder was performed for a simplified model. In

the model, Smith assumed incompressible air, no "splashing" of the liquid film, uniform mixture of the water droplets in the air stream, and a laminar boundary layer of the liquid film on the upstream side of the cylinder. The integral forms of the continuity, momentum, and energy equations were used to analyze the liquid film. Second order velocity and temperature profiles were assumed, but later were reduced to first order profiles. An expression for the local heat transfer coefficient as a function of known parameters was determined. Experimental data were reported at air free stream Reynolds numbers of 60,000 and 120,000 with water-air mass flow rate ratios varying from 0.016 to 0.088 and from 0.015 to 0.041, respectively. The analytical results agreed favorably with the experimental results. The cylinder temperature and the water droplet temperature were used in determining the temperature difference for the experimental heat transfer coefficients.

An analytical study published by Tifford (5) investigated the external heat transfer from a two-dimensional model exposed to a two-component flow. Tifford assumed laminar and incompressible flow, no pressure gradients, and no gravitational effects. He further assumed linear temperature and velocity profiles in the liquid film. The theoretical results were not verified with experimental results.

Goldstein, et al. (6) presented an analytical study of heat transfer and frictional effects of external two-component (gas-liquid) flow over a cylinder. He assumed uniform distribution of liquid droplets in the air stream, laminar and incompressible flow, and no gravitational effects. Evaporation of the liquid film was not considered. Waves and splashing by the liquid droplets in the liquid film on the cylinder sur-

face were neglected. Solutions were obtained in power series for the velocity and temperature profiles and for the Nusselt number. These results compared favorably with the experimental results of Acrivos. Goldstein assumed that the air and water spray were at the same temperature, while Acrivos' measurements indicated the air and spray water temperatures were different.

Purpose of Research

Experimental studies of external heat transfer from a heated cylinder exposed to two-component (air-water) crossflow are limited and conflicting. Neither Hoelscher (2) nor Acrivos (1) reported reliable data on the downstream side of the cylinder. Hoelscher (2) reported heat conduction inside the test cylinder resulting in negative heat transfer coefficients on the downstream side of the cylinder. Since the heat transfer coefficients reported by Acrivos (1), Hoelscher (2), and Takahara (3) were higher than the maximum possible sensible heating of the liquid film, evaporation of the liquid film must have occurred. Acrivos (1), Hoelscher (2), Takahara (3), and Smith (4) reported no data with the air saturated prior to the injection of the water spray droplets.

Therefore, it was the intention of this investigation to determine experimentally the local and overall Nusselt numbers for an isothermal cylinder exposed to two-component (air-water) crossflow. The effects of the air free stream Reynolds number and the water-air mass flow rate ratio on the Nusselt numbers were studied. This study included only the situation with a non-evaporating film on the cylinder surface exposed to saturated air with entrained water droplets. Air free stream Reynolds

numbers of 30,000, 75,000, and 118,000 and water-air mass flow rate ratios varying from 0.012 to 0.13 were considered.

CHAPTER II

EQUIPMENT AND INSTRUMENTATION

A test facility was constructed to study the local and overall heat transfer characteristics of an isothermal cylinder exposed to two-component (air-water) crossflow. The apparatus consisted of a two-component flow closed loop wind tunnel, an internally heated circular cylinder, a water spray system, and temperature and power measuring equipment.

Governing Equation

The equation used to determine the local Nusselt numbers across the water and air boundary layers from the experimental data was

$$Nu_{Dw}\Big|_{\theta} = \frac{D\, Q_s}{k_w A_s (T_s - T_\infty)}$$

where

$Nu_{Dw}\Big|_{\theta}$ = local Nusselt number, $\frac{h\, D}{k_w}$

D = cylinder diameter

Q_s = power output by a cartridge heater

k_w = thermal conductivity of the water

A_s = 1/12 of the total surface area of the test section

T_s = local cylinder surface temperature

T_∞ = free stream reference temperature

In the experiments, the water spray temperature and the air wind tunnel dry bulb temperature were approximately identical. The water spray

temperature was used as the free stream reference temperature. The air in the wind tunnel was saturated during the heat transfer experiments. The cylinder surface was maintained isothermally by adjustments of the power input to the heaters. The overall Nusselt number was determined from the local Nusselt numbers.

Equipment

Wind Tunnel

A closed loop wind tunnel was designed, constructed, and calibrated to produce two-component (air-water) flow in the vertical test section area (Figure 1). Air velocities in the test section area, ranging from 15 to 100 feet per second, were obtained by using a 6000 cfm industrial fan (American-Standard Industrial Division) driven by a 15 horsepower electric motor. The air velocity was controlled by a damper located on the exhaust side of the fan. The wind tunnel air was saturated (90 to 98 per cent relative humidity) during the experiments. The wind tunnel was constructed in units of 1/4 and 1/2-inch thick Marine Grade "A-A" plywood and bolted together with aluminum flanges. The plywood was treated with a wood sealer and a Poly-urethane varnish, which resulted in a very smooth protective finish on the inside walls of the wind tunnel.

The wind tunnel will be divided into four areas for further discussion.

Test Section Area. The test section area, with a 12-inch by 12-inch cross-section, was designed vertically, instead of horizontally, to minimize the effects of gravity on the water spray droplets. Acrivos (1) reported that while using a horizontal test area, the water droplets began

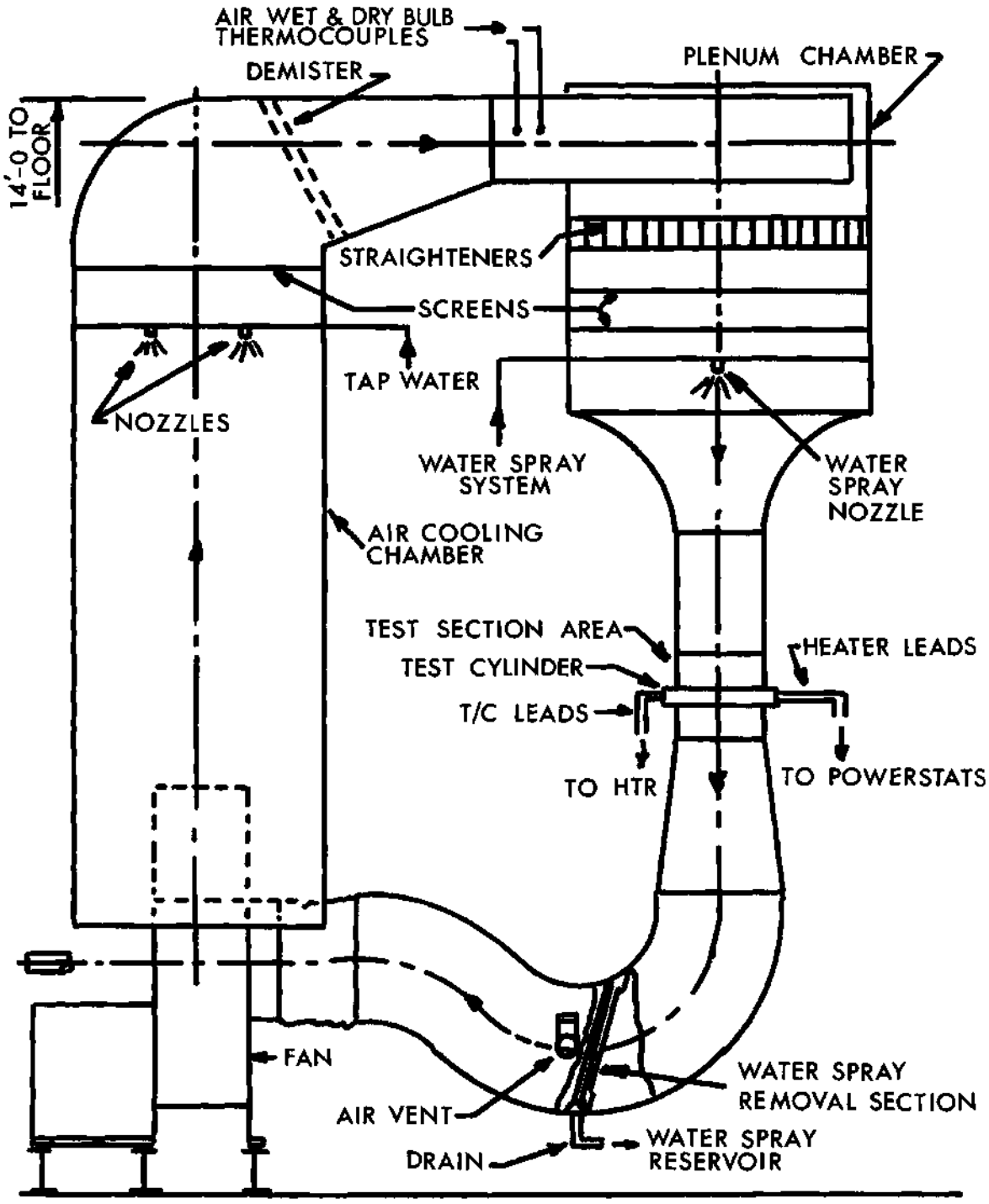

Figure 1. General Arrangement of Two-Component (Air-Water) Flow Wind Tunnel.

to fall out of the air stream at air velocities below 50 feet per second. Also, water running off other sections of the test cylinder onto the test section could be minimized. The walls were made of clear Plexiglas so visual observations could be made during tests. The cylinder test section was mounted horizontally through the Plexiglas walls. The pitot-static probe and the spray droplet distribution apparatus were located in this area, upstream of the cylinder.

Water Spray Removal Section. Downstream of the test section area, a water spray removal system was installed to recapture the water spray. This allowed the same water spray to be recycled, thus lowering the heat load necessary to maintain a desired temperature for the water spray. The water droplets were thrown out of the air stream and onto the walls by means of an 18-inch by 18-inch ninety degree elbow. Four $1\frac{1}{2}$-inch by $1\frac{1}{2}$-inch aluminum angles were mounted on the walls, one on each wall, and $\frac{1}{2}$-inch slots were cut on the upstream side of the angles. As the water ran down the wind tunnel walls, the angles trapped the water and channeled it to the drain. A drain was provided to return the water to the water spray reservoir. It was necessary to install an air vent to prevent the water in the reservoir from being pulled back through the drain into the wind tunnel. The fan and damper were located between the water spray removal section and the air cooling chamber.

Air Cooling Chamber. A vertical chamber, 36-inches by 36-inches in cross-section, was provided on the outlet side of the fan. In this low velocity chamber, a direct air-water counterflow cooling system was installed. By using tap water and two high capacity nozzles, sufficient cooling capacity was provided to control the air temperature. Across the

top of the chamber was placed a 16 x 18 gage aluminum screen which provided a method to separate the large water droplets from the air stream. Next, a one-inch thick demister (a device to separate liquid droplets from a gas stream) was installed to collect most of the remaining water droplets borne by the air stream. An elbow section was provided to connect the air cooling chamber with the plenum chamber. In this elbow section, the air dry and wet bulb temperatures were determined.

Plenum Chamber. A vertical chamber, 44-inches by 44-inches in cross-section, was provided to stabilize the air before it entered the test section area. Aluminum straighteners and two 16 x 18 gage aluminum screens were installed across the chamber to dampen out pressure gradients and reduce velocity fluctuations in the air flow. The nozzle was mounted below the screens to provide the water spray for the two-component flow. An aluminum converging nozzle was provided to connect the plenum chamber with the test section area.

Water Spray System

A water spray system was designed and installed to provide the necessary spray distribution in the test section area (Figure 2). The spray nozzle was installed in the plenum chamber, below the screens and 53-inches above the test cylinder. The nozzle was located in the plenum chamber to insure better water droplet distribution as reported by Brun (7). An SQ-10 nozzle, furnished by the Delavan Manufacturing Company, was used to provide the water spray for the two-component flow. The nozzle provided a relatively uniform, square shaped water spray distribution. For several of the experiments, a second SQ-10 nozzle was located six-inches directly below the first nozzle so higher water-air mass flow rate ratios

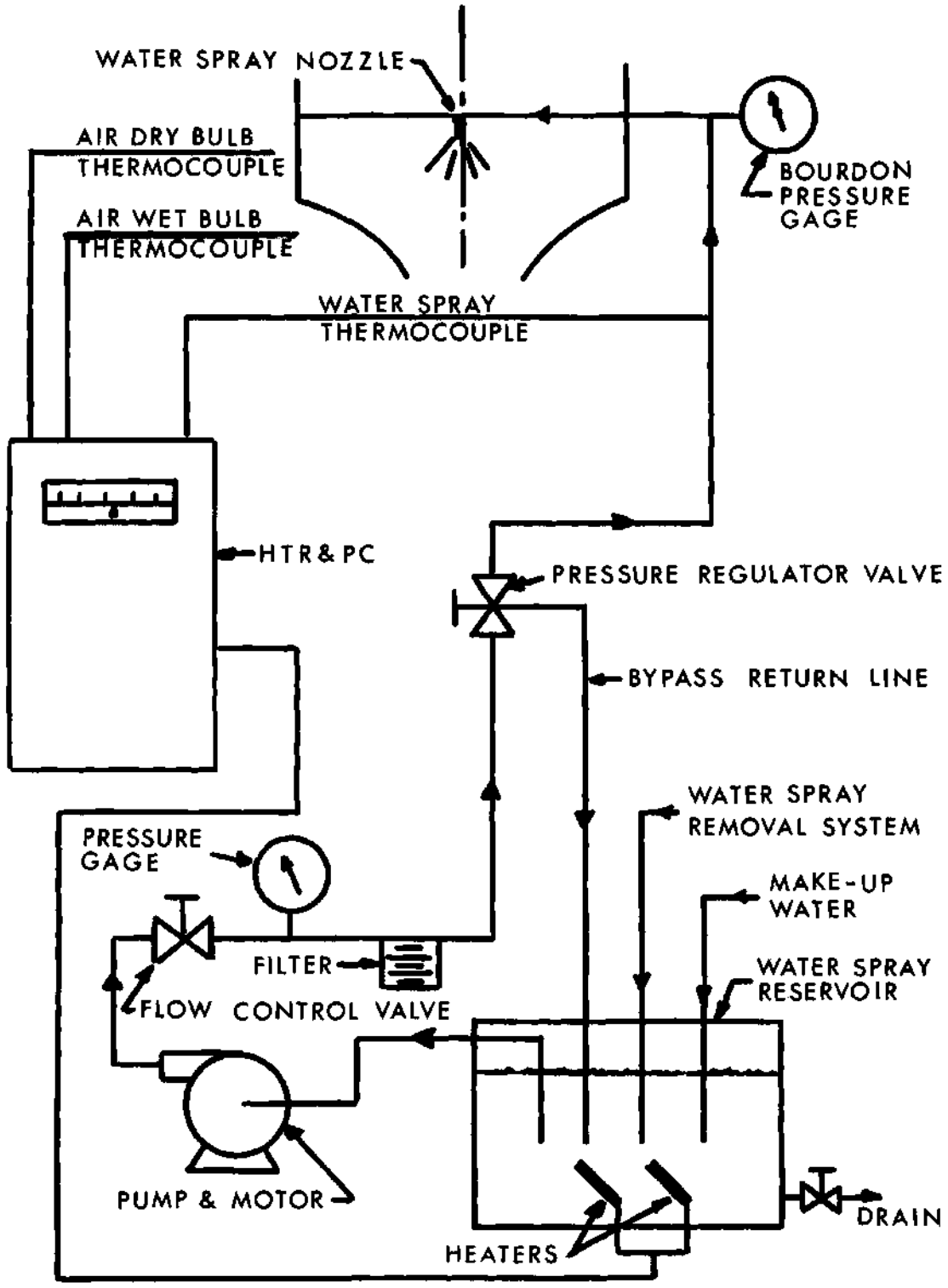

Figure 2. Water Spray System.

could be obtained.

A fifteen-gallon tank was used as a water spray reservoir. Two thermocouples were installed in the water spray line just prior to the spray nozzle. One of the thermocouples was connected to a Honeywell temperature recorder and power controller (HTR & PC) and the other thermocouple was connected to a 20 channel Honeywell temperature recorder (HTR). The HTR & PC was used to monitor the air dry and wet bulb temperatures (see page 17) and the water spray temperature. The variable power output on the HTR & PC was connected to the reservoir heaters and adjusted so the water spray temperature was equal to the air dry bulb temperature.

A turbine pump, furnished by the Aurora Pump Company (Model No. TS-E5T-1) and driven by a three-horsepower motor, was used to supply the high pressure water spray. A flow control valve and a high pressure regulator valve, with a bypass return line to the reservoir, were used to control the water spray flow rate. A Bourdon pressure test gage was used to indicate the water spray pressure at the nozzle.

Test Cylinder

A three-inch diameter cylinder, divided into five main sections and mounted horizontally in the test section area, was used for the experiments. Located in the middle of the cylinder was a four-inch long brass test section used for the heat transfer studies (Figure 3). To eliminate longitudinal heat flow and end effects, a three-inch long Teflon guard section was mounted on either side of the brass test section. On either side of the Teflon guard sections was mounted a three-inch long aluminum pipe section for support. On each end of the aluminum pipe sections was a cap plate. A bolt ran through the center of the entire cylin-

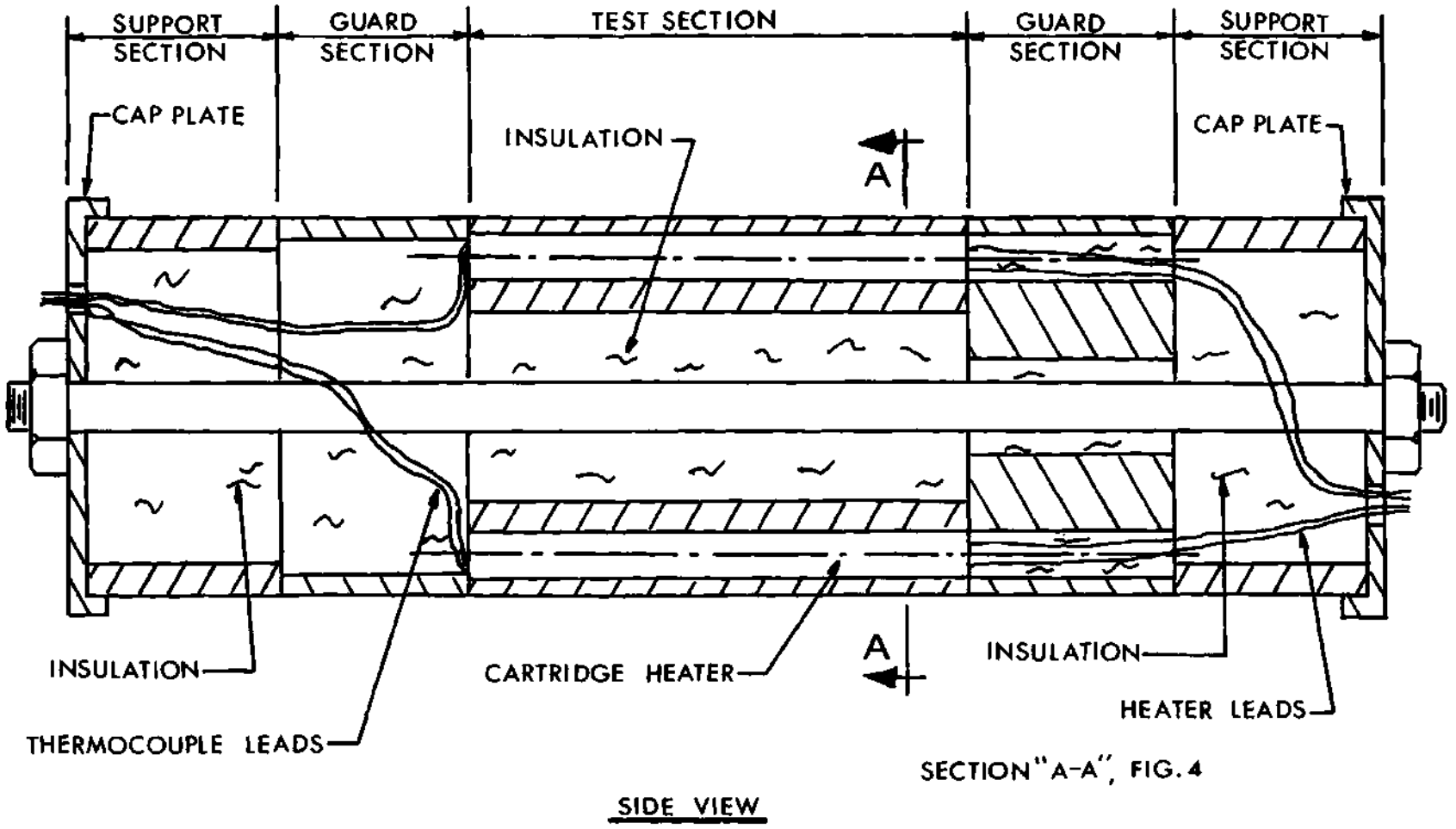

Figure 3. Test Cylinder.

der to hold it together.

The brass test section was divided into twelve equal but separate heater sections, with a 3/8-inch diameter chamber in each section. The isolated 30 degree heater section provided a means to study the local heat transfer effects. Watlow Firerod cartridge heaters were installed in each heater section chamber, with the heater power output varying from 500 watts on the upstream side to 125 watts on the downstream side of the cylinder (Figure 4). The cylinder was drilled out to an $1\frac{1}{2}$-inch inside diameter and radial slots, 1/16-inch wide and cut to within 1/16-inch of the cylinder surface, were made to provide essentially separate heater sections. The slots and the inside sections of the cylinder were filled with Santocel "A" insulation (Monsanto Chemical Company).

Thermocouples were mounted on the periphery of the brass test section. Longitudinal slots on isothermal lines, 1/16-inch wide, 1/16-inch deep, and two-inches long, were cut on the cylinder surface on the centerline of each heater section (Figure 4). Two additional slots, equally spaced 1/4-inch off center of a main longitudinal slot, were cut. This provided a means to determine if the cylinder surface temperature varied circumferentially in a heater section. The slots were tinned with soft solder, then the thermocouples were placed in the slots with the thermocouple junction located on the cylinder surface at the cylinder centerline. Then solder was used to fill in the remainder of the slot. Emery cloth was used to restore the cylinder surface to a smooth finish. The cylinder surface was washed in a solution of warm water and a mild detergent to remove all grease and insure good wetting characteristics.

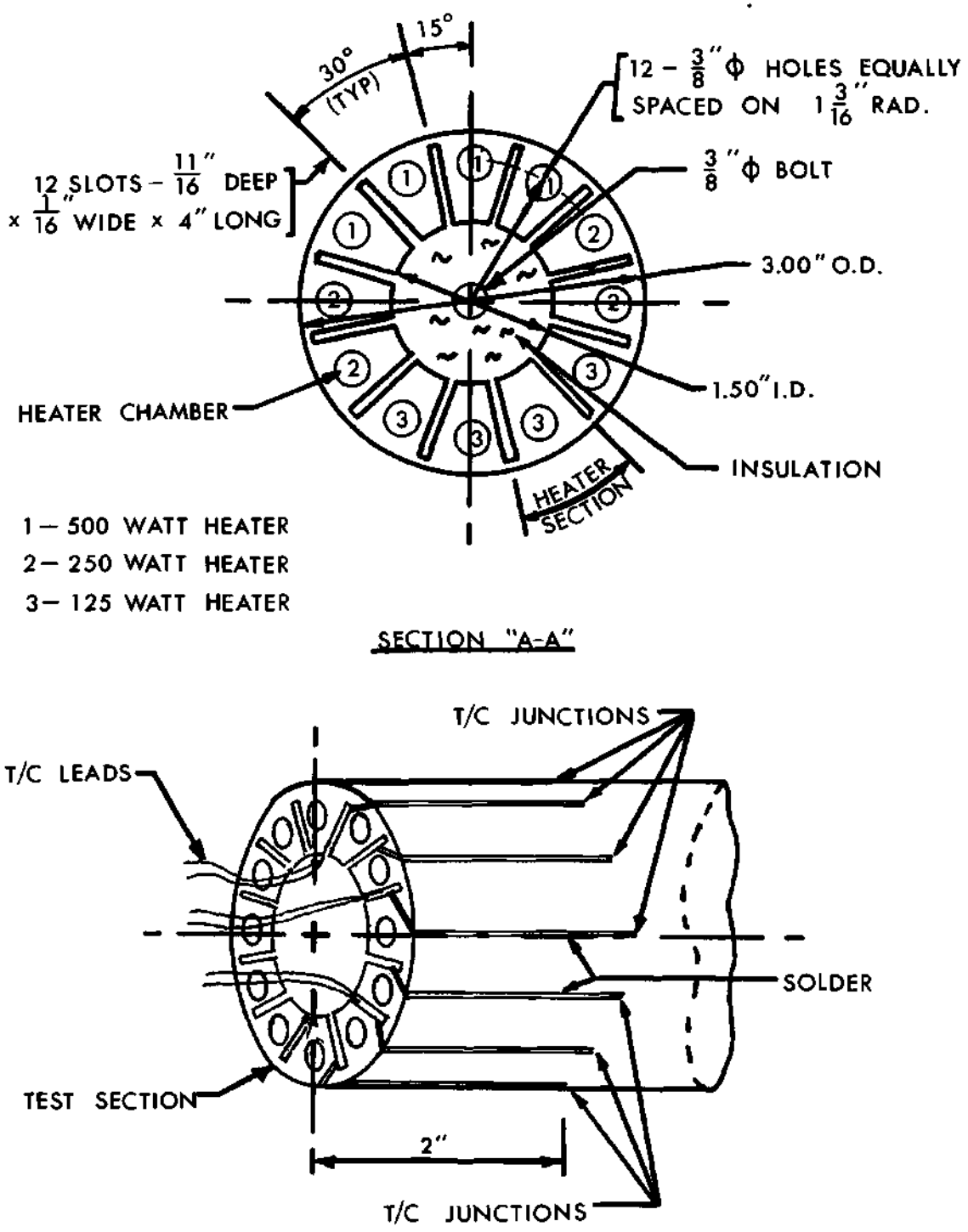

Figure 4. Test Cylinder.

Instrumentation

Temperature Measurements

During heat transfer tests, it was necessary to determine and record the local cylinder surface temperatures, the water spray temperature, and the air dry and wet bulb temperatures. These temperatures were monitored on the HTR & PC and/or on the HTR (Figure 5). The fourteen cylinder surface thermocouples, a water spray thermocouple, and an air dry bulb thermocouple were connected to the HTR. The air wet bulb thermocouple, the other water spray thermocouple, and the other air dry bulb thermocouple were connected to the HTR & PC. The cylinder surface thermocouples were made from 30 gage Teflon coated copper constantan thermocouple wire. The two air dry bulb thermocouples, the two water spray thermocouples, and the air wet bulb thermocouple were made from 24 gage copper constantan thermocouple wire. Two dewar vacuum flasks containing a mixture of crushed ice and water were used for the HTR reference junction. To obtain reliable temperature measurements a potentiometer (Leeds and Northrup Co.,Model No. 8686), connected into the HTR, was used during heat transfer tests to measure the emf generated by the fourteen cylinder thermocouples, the air dry bulb thermocouple, and the water spray thermocouple.

The wind tunnel air dry and wet bulb thermocouples were located in the elbow section connecting the air cooling chamber with the plenum chamber. The junctions of the air dry bulb thermocouples were located in a modified deceleration probe to insure against water droplets coming into contact with the junctions (Figure 6). The air wet bulb thermocouple was made of five thermocouple junctions, connected in parallel and each junction covered with a cloth wick which was partially submerged in water.

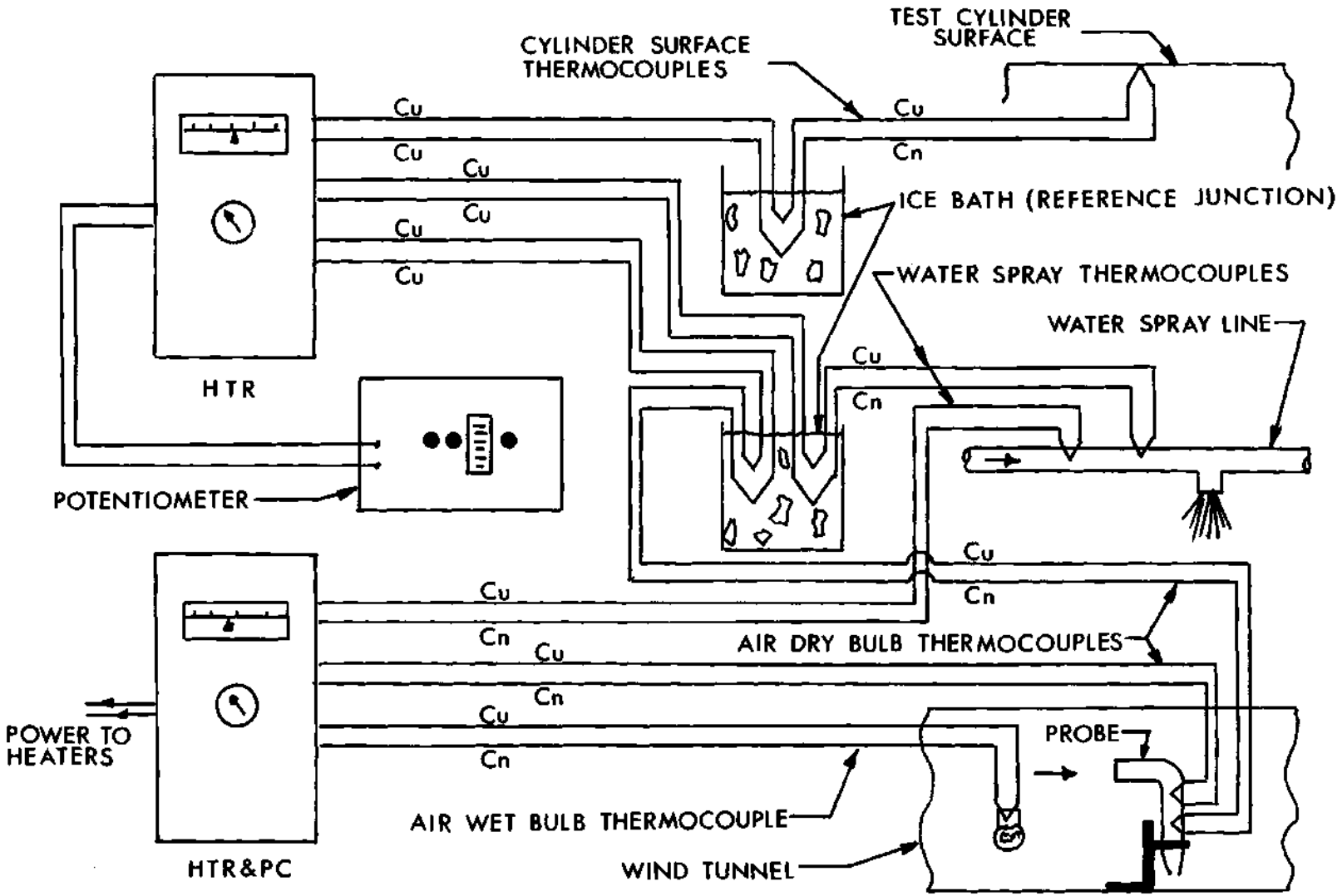

Figure 5. Schematic of Thermocouple Layout.

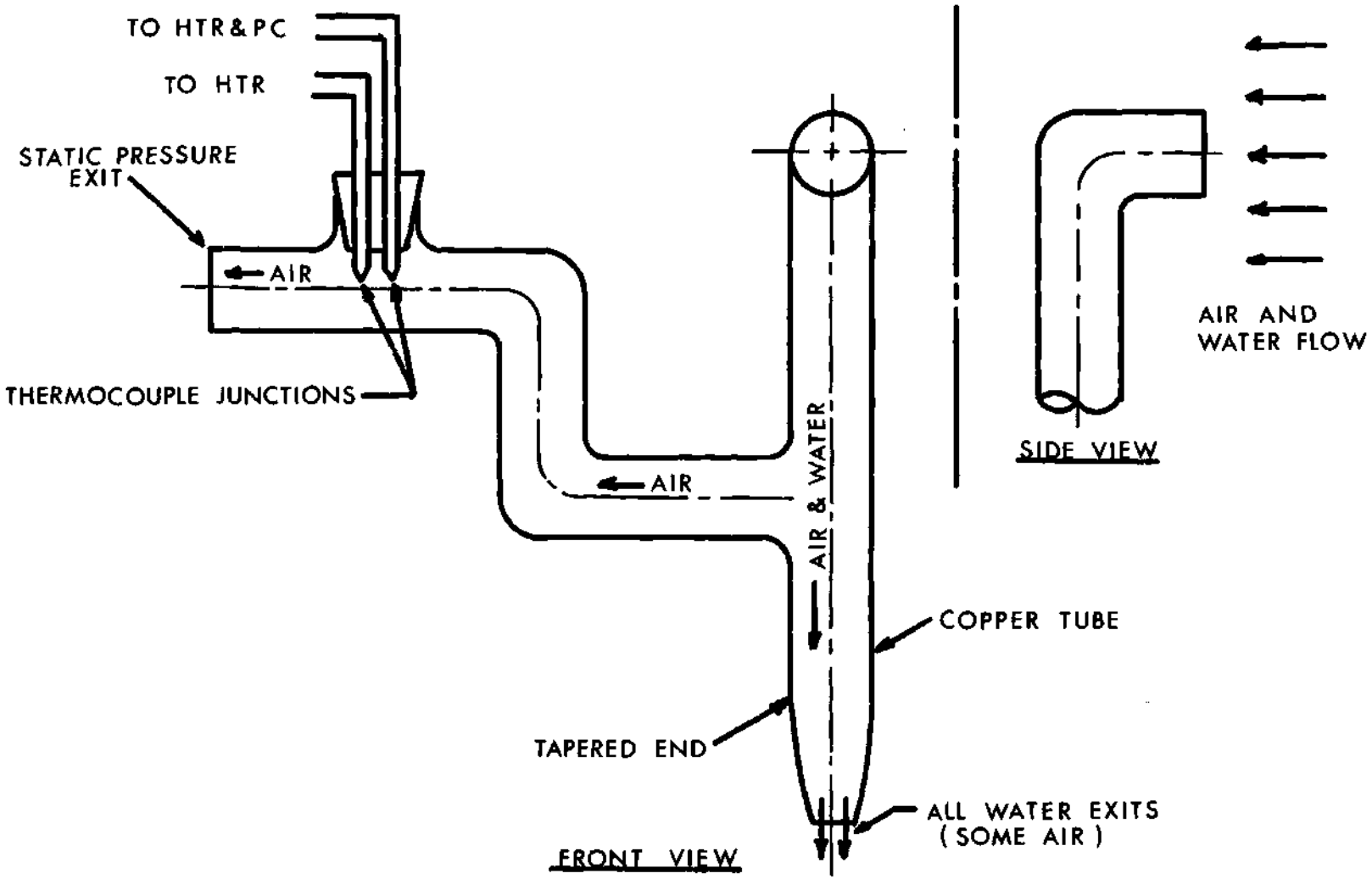

Figure 6. Air Dry Bulb Temperature Probe.

The water spray thermocouples were installed in the water spray line just prior to the spray nozzle in the plenum chamber.

Power Measurements

The power input to the heaters was determined by measuring the heater current and voltage on a wattmeter (Weston, Model 310, single phase, 1 ampere). A diagram of the electrical layout is shown in Figure 7. The power input to each heater was measured to determine the local heat dissipation. By adding all the local power inputs, the total heat dissipation was determined. A Powerstat variable transformer was connected to each heater so an isothermal cylinder surface could be obtained by adjusting the transformers. A Sorenson power regulator was provided for each set of six cartridge heaters.

Pressure Distribution Around the Cylinder

Two-Component (Air-Water) Flow. A system to measure the pressure distribution on the upstream side of the cylinder in two-component (air-water) flow was constructed. A three-inch diameter clear Plexiglas cylinder with a 1/32-inch diameter pressure tap was used for the tests. Good cylinder surface wetting characteristics were obtained by finishing the surface with fine Emery cloth. The pressure tap was connected to a vertical glass tube located outside the wind tunnel. The entire system was filled with manometer fluid.

One-Component (Air) Flow. The pressure distribution around the cylinder in one-component flow was determined. The same cylinder used in the two-component pressure distribution system was used except the cylinder pressure tap was connected to a micromanometer (Merian, ten-inch, Model No. 34F82).

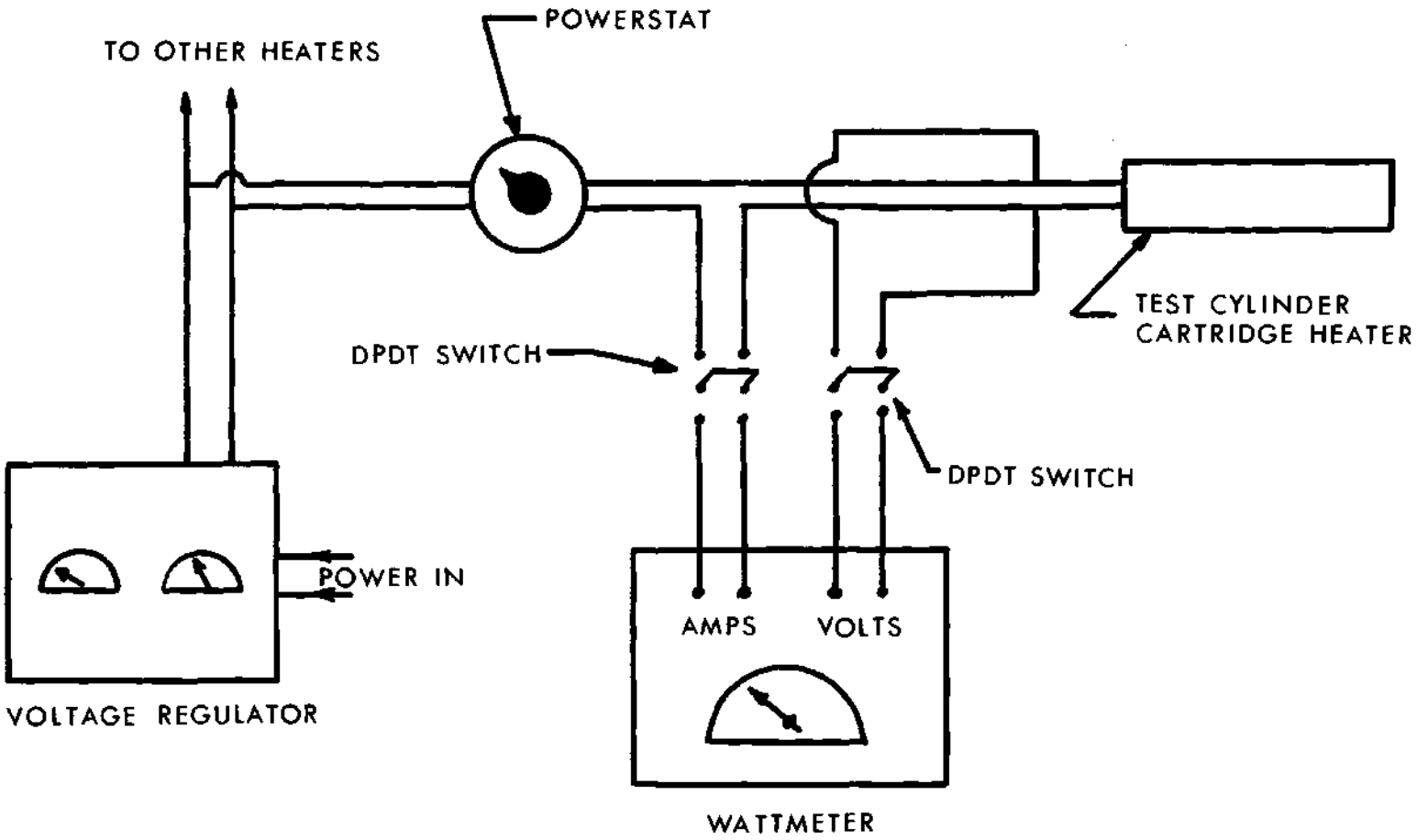

Figure 7. Electrical Circuit for Test Cylinder Cartridge Heaters.

Spray Droplet Distribution and Water Mass Flow Rate Determination

A continuous sampling method, similar to that described by Dussourd (8), was used to determine the distribution and the mass flow rate of the water droplets at the vertical test section area (Figure 8). Three 0.228-inch inside diameter thin-walled brass probes, spaced two-inches apart and mounted on a horizontal traverse, were used to capture the droplet laden air. Since Smith (4) had shown that the diameter of the water spray probe resulted in less than ± 3 per cent variation in water collection rate, only one size probe was used. Each probe was connected to a 25 ml graduated burette where the water was collected and separated from the air. The air was then returned to the wind tunnel at static pressure.

Air Velocity

The air velocity in the test section during one-component (air) flow was determined with a 1/32-inch outside diameter pitot-static probe located at the wind tunnel centerline seven-inches upstream from the test cylinder stagnation point. The pitot-static probe was connected to the micromanometer.

Spray Droplet Velocity

Tests were performed to determine the average water droplet velocity by the method of "droplet impact pressure" as described by Dussourd (8) and Sucec (9). A thin-walled glass probe (1/4-inch inside diameter) was mounted on the horizontal traverse and located eight-inches upstream from the test cylinder stagnation point. The probe was connected to a vertical glass tube located outside the wind tunnel. The entire probe system was filled with water containing a colored dye and a wetting agent. A cathetometer (Gaertner Scientific Corp., Model No. 463A) was used to

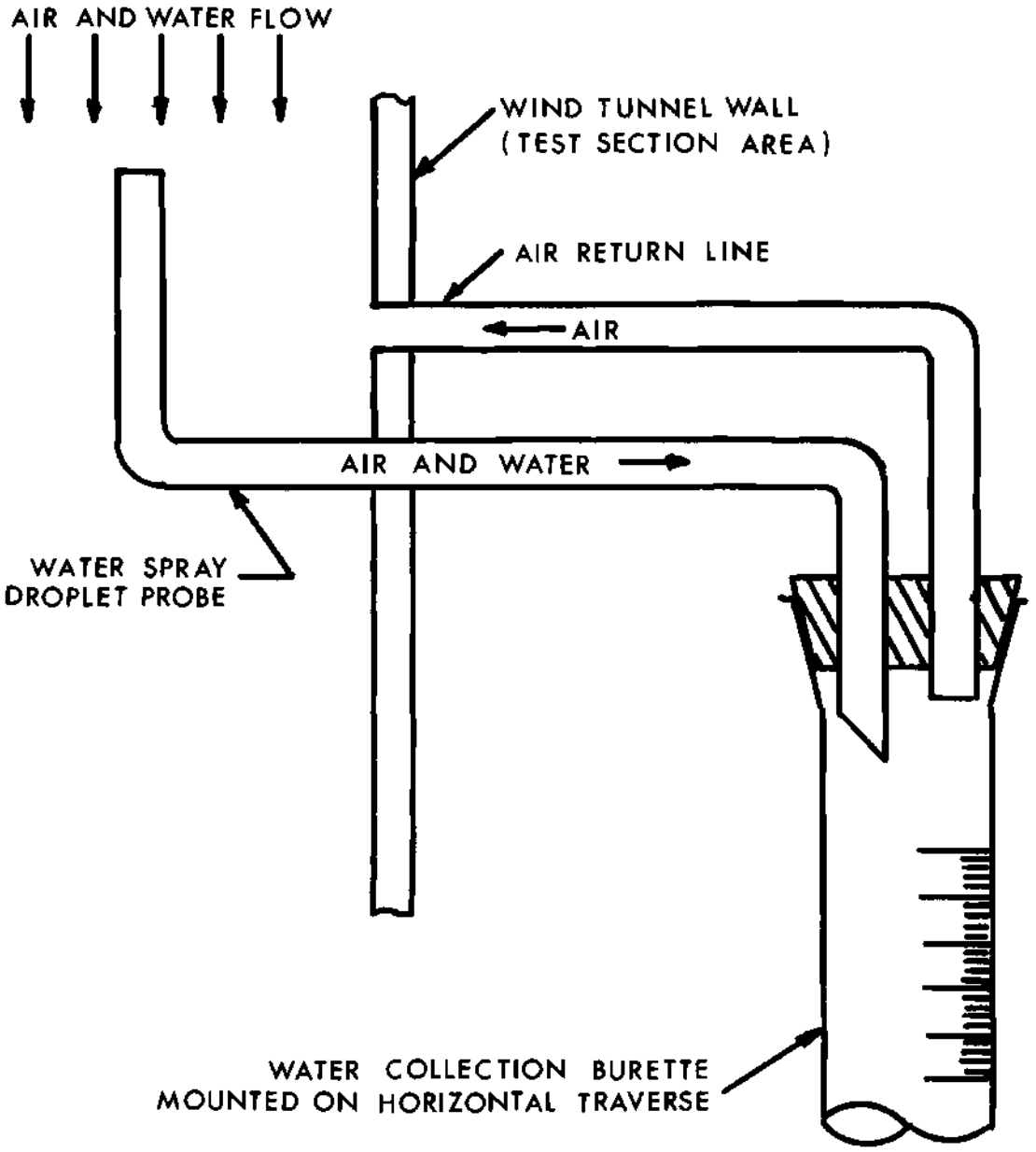

Figure 8. Probe for Spray Droplet Distribution and Water Spray Flow Rate Determination.

determine the manometer fluid height difference in stagnation pressure for the air flow and for the combined air-water flow.

CHAPTER III

CALIBRATION AND PROCEDURE

Calibration

In this section a discussion is given of the calibration of the wind tunnel which includes determining the air velocity characteristics in one-component (air) flow and the water spray droplet characteristics in two-component (air-water) flow. Calibration of the test cylinder surface thermocouples and the wattmeter and determination of the pressure distribution around the cylinder is also presented. An error analysis of the local Nusselt number and the water-air mass flow rate ratio is developed.

Wind Tunnel

Air Velocity Profile. Air velocity profiles for 20, 50, and 80 feet per second were made in the test section area. These profiles were determined by using a 1/8-inch outside diameter pitot-static probe and the micromanometer. These tests were performed with the pitot-static probe occupying the test cylinder's place in the test section area. Air velocity measurements were made at one-inch intervals across the wind tunnel. The velocity variations at 20, 50, and 80 feet per second were 0.0, 0.0, and + 0.5 feet per second, respectively. The velocity profiles are shown in Figure 9.

Air Dry Bulb and Water Spray Thermocouples. The air dry bulb thermocouple and the water spray thermocouple which were connected to the

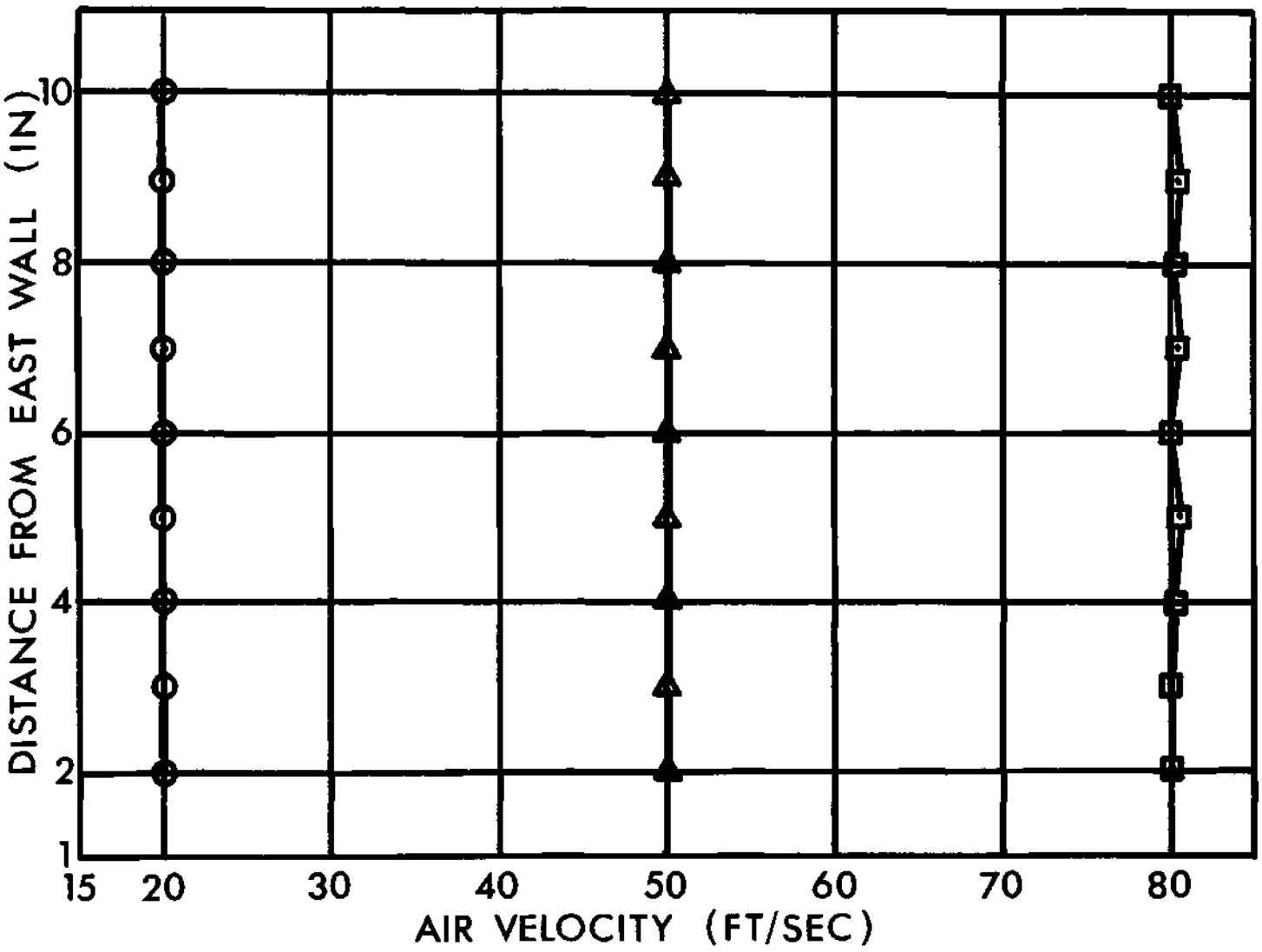

Figure 9. Velocity Profile Along Test Cylinder Centerline.

HTR were calibrated against a mercury-in-glass thermometer (Fisher Scientific Co., Model No. 15-043C). A water-ice ($32^{o}F$) reference junction was used and a potentiometer (Leeds and Northrup Co., Model No. 8686) was used to measure the thermocouple emf. The thermocouples were calibrated from 70 to $110^{o}F$ in $10^{o}F$ intervals. The air dry bulb thermocouple temperature varied a maximum of $-0.9^{o}F$ from the comparison thermometer temperature. The spray water thermocouple temperature varied a maximum of $-0.6^{o}F$.

Spray Droplet Distribution. Spray droplet distribution tests were performed with the test cylinder in the test section area and the collection probes located eight-inches upstream from the stagnation point of the cylinder. The nozzle was centered in the plenum chamber and aligned so that it would spray vertically, by directing a Strobotac light onto the water spray cone at the nozzle. Traverses with the three collection probes were made, starting at 4.5-inches from the wind tunnel wall and moving four times in 0.75-inch increments across the projected area of the cylinder test section. During the heat transfer tests, the spray droplet distribution varied from ± 16 to ± 45 per cent from an average water mass flow rate. Results of two particular runs are shown in Figures 10 and 11.

Tests were conducted to determine the repeatability of the average water mass flow rate during tests for the Reynolds numbers of 30,000 and 118,000. At both Reynolds numbers, the average water mass flow rates recorded for the first and second traverses varied less than five per cent.

Median Water Spray Droplet Diameter. The nozzle vendor, the Delavan Manufacturing Company, was contacted to determine the mass median

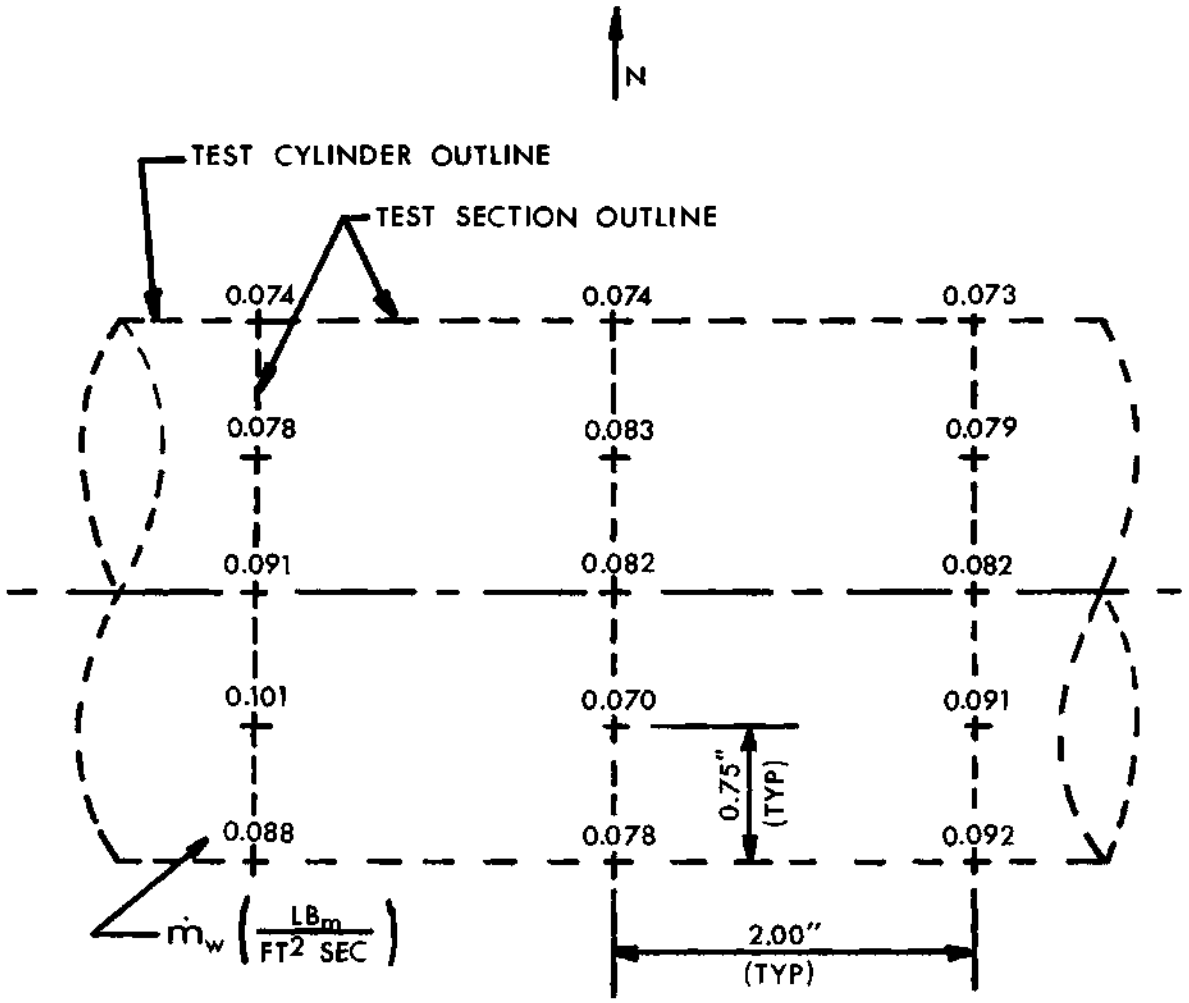

AVG. $\dot{m}_w = 0.081 \frac{LB_m}{FT^2\ SEC}$

DEVIATION FROM AVG. $\dot{m}_w = \begin{cases} +13\% \\ -11\% \end{cases}$

Figure 10. Water Spray Droplet Distribution; Re = 30,000, $\bar{m}$ = 0.056.

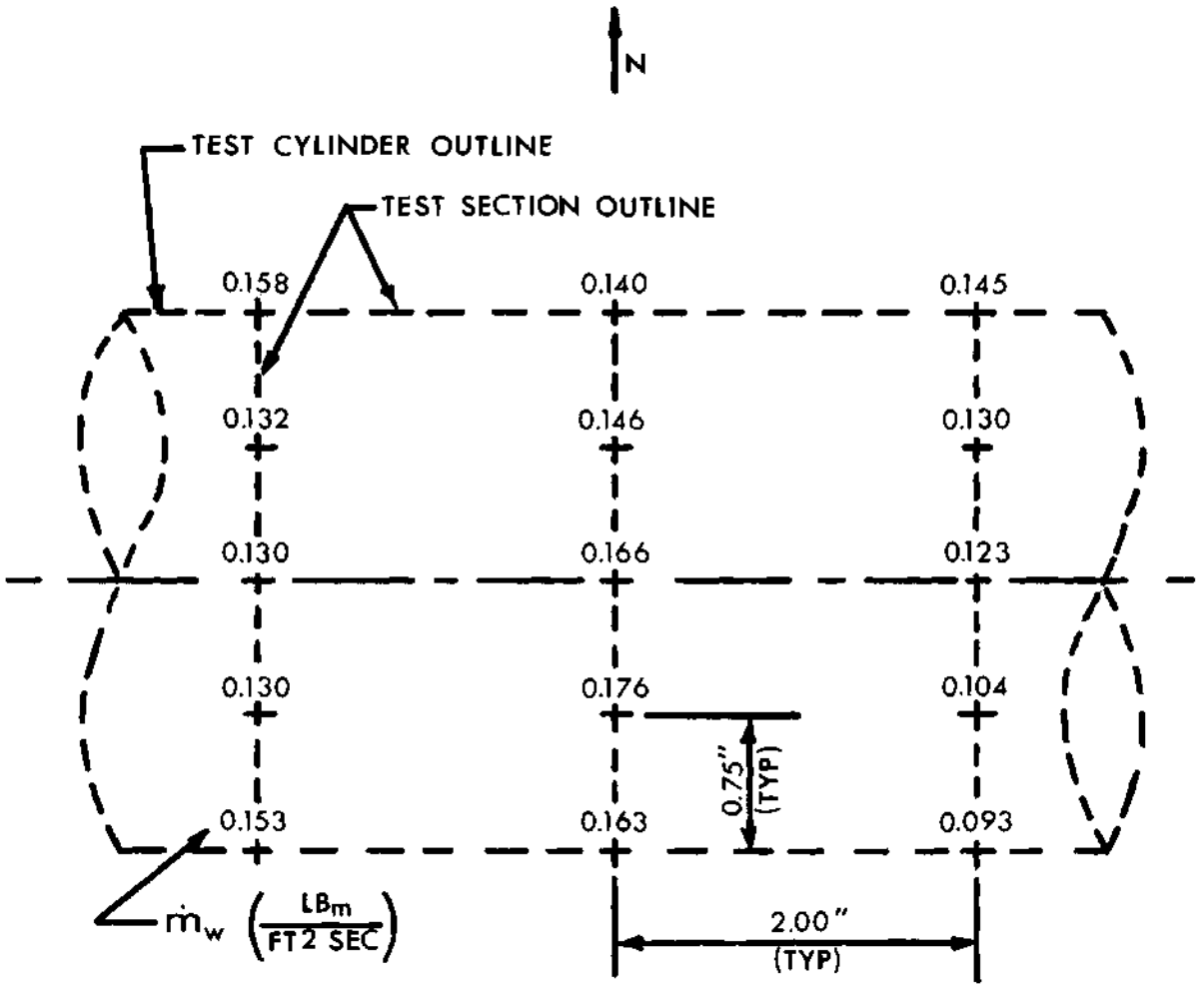

AVG. $\dot{m}_w = 0.135 \frac{LB_m}{FT^2\ SEC}$

DEVIATION FROM AVG. $\dot{m}_w = \begin{cases} +28\% \\ -31\% \end{cases}$

Figure 11. Water Spray Droplet Distribution; Re = 118,000, $\bar{m}$ = 0.024.

water droplet diameter. The water droplet size distribution and the mass median water droplet diameter for an SQ-10 nozzle operating at 40 and 200 psig without air flow were measured. From these data, a plot of mass median water droplet diameter versus the nozzle supply pressure (Figure 12) was determined. The mass median water droplet diameter decreased as the nozzle pressure increased. The effect of spray injection into the moving air stream and the effect of the wind tunnel characteristics on the water spray droplet size were unknown.

Average Water Spray Droplet Velocity. Tests were conducted to determine the average water spray droplet velocity in the test section area at air free stream Reynolds numbers of 30,000, 75,000, and 118,000, and at different water-air mass flow rate ratios. A method described by Dussourd (8) was used. From the equation

$$P_{STAGN}\Big|_{a-w} = P_{STAGN}\Big|_{a} + \left(\frac{\dot{m}_w}{g_c}\right)\left(U_\infty\right)\left(\bar{e}_p\right)$$

the water droplet velocity was determined, assuming total conversion of the water droplet momentum into pressure upon contact with the water in the probe. The probe efficiency ($\bar{e}_p$) was assumed equal to one. The combined air-water stagnation pressure was determined during two-component flow. Then by determining the air stagnation pressure in one-component flow and the water mass flow rate, the average droplet velocity was calculated.

The average spray droplet velocity was 250 feet per second with a ± 15 feet per second variation for a Reynolds number of 30,000 and for water-air mass flow rate ratios varying from 0.025 to 0.053. At the

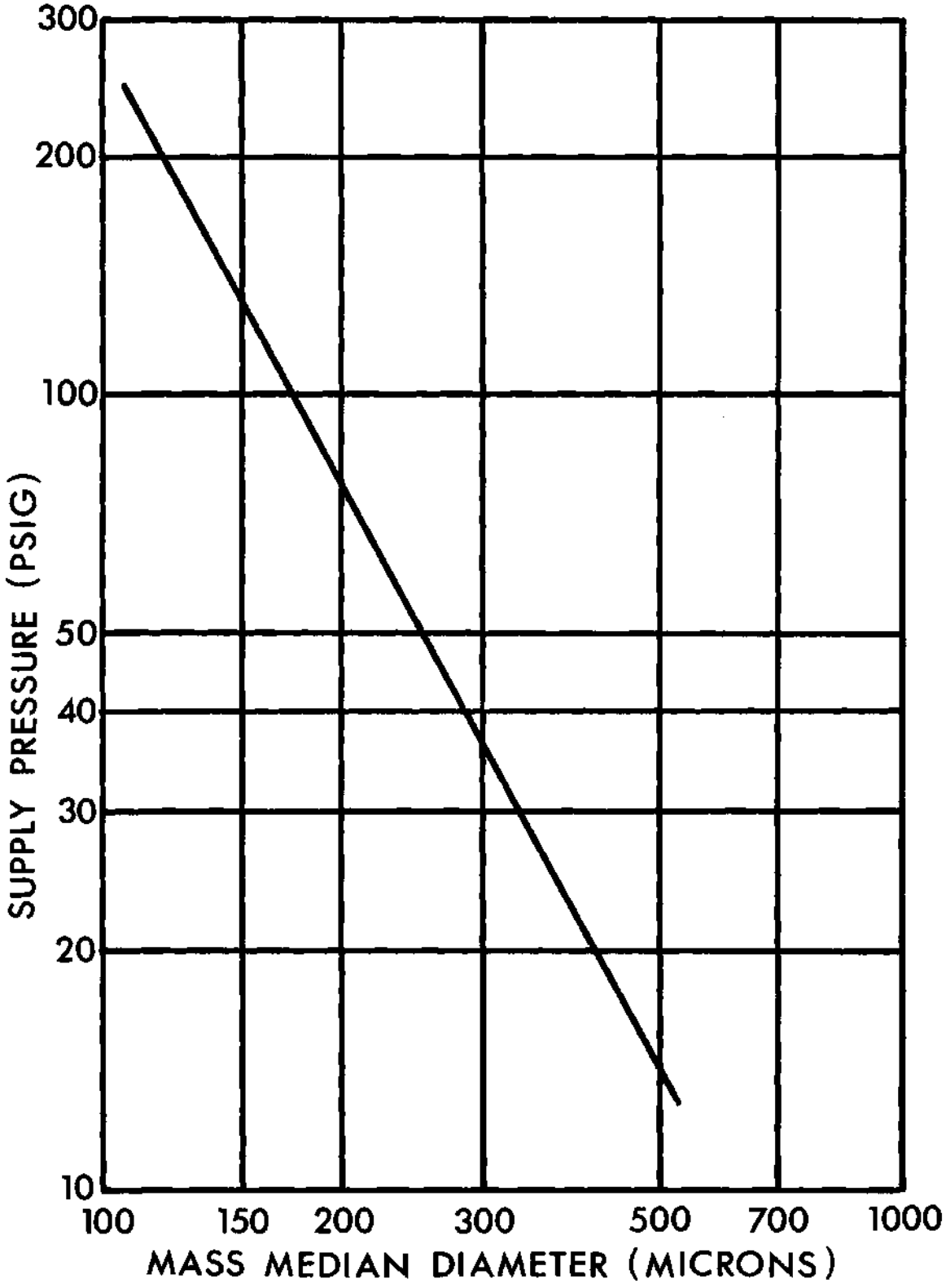

Figure 12. Mass Median Droplet Diameter versus Supply Pressure.

Reynolds number of 75,000, the average spray droplet velocities were 43, 84, and 118 feet per second at water-air mass flow rate ratios of 0.013, 0.029, and 0.053, respectively. For a Reynolds number of 118,000 and on separate runs, average spray droplet velocities of 95 and 255 feet per second at water-air mass flow rate ratios of 0.038 and 0.024, respectively, were recorded.

The spray droplet velocities of 250 and 255 feet per second corresponding to nozzle pressures varying from 100 to 220 psig seemed to be in error, since the average velocity for the nozzle pressure of 220 psig was only 180 feet per second.

Test Cylinder

Cylinder Thermocouples. The test cylinder surface thermocouples were calibrated against the mercury-in-glass comparison thermometer in a thermometer-comparison water bath (Precision Scientific Co., Model No. 66580). The cylinder was placed vertically in the bath with the brass test section submerged and the comparison thermometer completely submerged. A water-ice ($32^{\circ}F$) reference junction was used and the potentiometer was used to measure the thermocouple emf. The fourteen thermocouples were calibrated from 70 to $150^{\circ}F$ in $10^{\circ}F$ intervals. The thermocouple temperatures were within $\pm 0.5^{\circ}F$ of the comparison thermometer temperatures.

Wattmeter. The wattmeter used to determine the cartridge heater wattage was calibrated using a precision resistor and a Standard voltage cell in a potentiometer. The Standard voltage cell had been calibrated against a National Bureau of Standards voltage cell. The wattmeter read within the limits of the factory calibration, $\pm$ 1/4 of one per cent of

full scale reading. Therefore, the wattmeter readings were accurate within ± 0.30 watts.

Pressure Distribution Around the Cylinder. Tests were performed to determine the pressure distribution around the Plexiglas cylinder in one-component (air) flow and two-component (air-water) flow for the Reynolds numbers of 30,000, 75,000, and 118,000. The results for one-component flow are shown in Figure 13 and are compared with results published by Fage and Falkner (10). The results of the pressure distribution on the upstream side of the cylinder for two-component flow are presented in Figure 14. At the Reynolds number of 75,000, runs at two different water-air mass flow rate ratios were performed to determine the effects of the water flow rate on the pressure distribution. From this test, the variation in water flow rate had no effect on the pressure distribution. The pressure distribution agreed very favorably with the solution obtained for potential flow around the cylinder with no water droplets in the air stream. The tests at the Reynolds number of 30,000 proved unsuccessful since the error involved was much greater than the pressures which were measured.

Experimental Error Analysis

An error analysis of the experimental data for the Nusselt number and the water-air mass flow rate ratio was performed.

Considering the Nusselt number,

$$Nu_{Dw|\theta} = \left(\frac{D}{k_w}\right)\left(\frac{Q_s}{A_s\ (T_s - T_\infty)}\right)$$

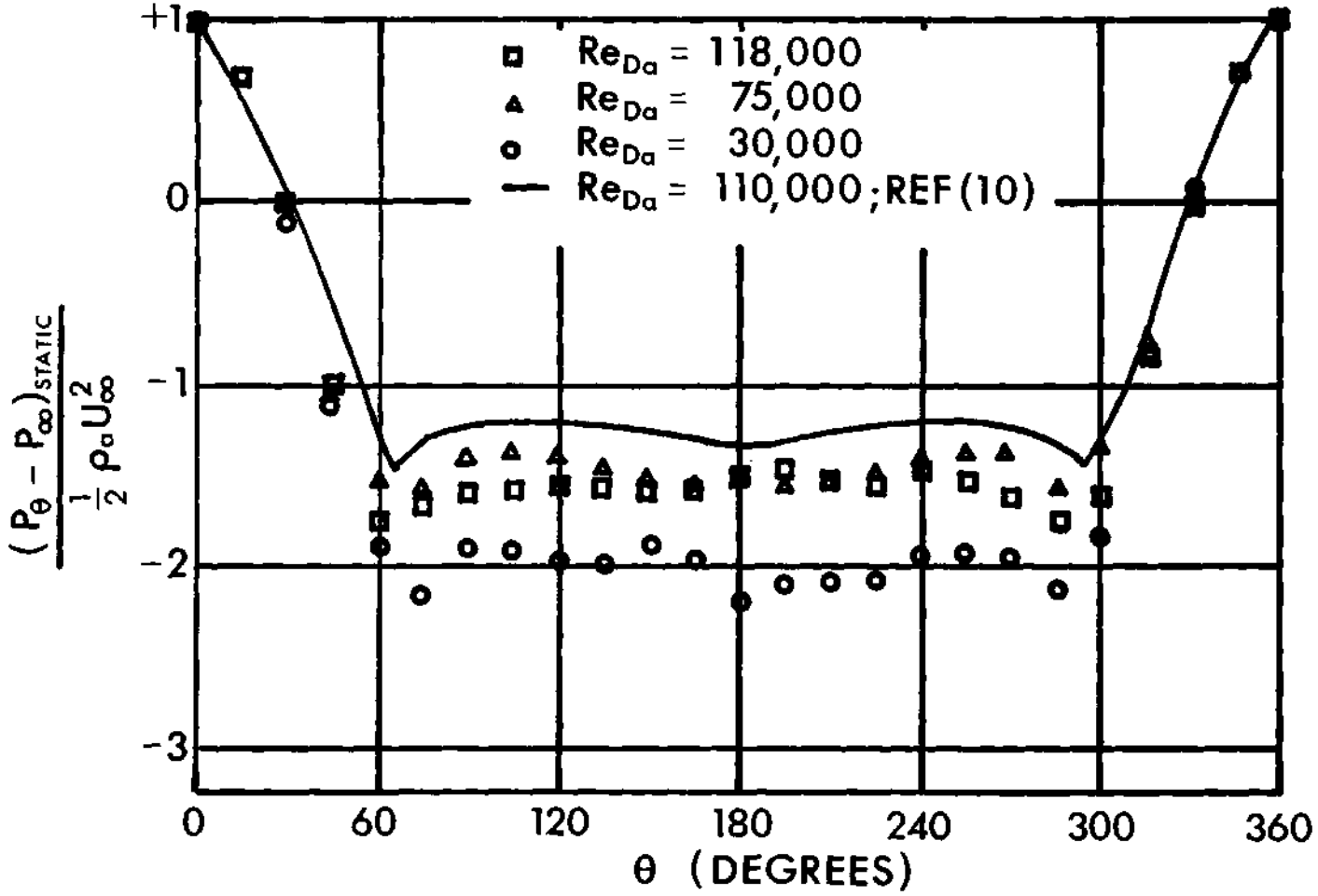

Figure 13. Pressure Distribution Around Plexiglas Cylinder in One-Component (Air) Flow.

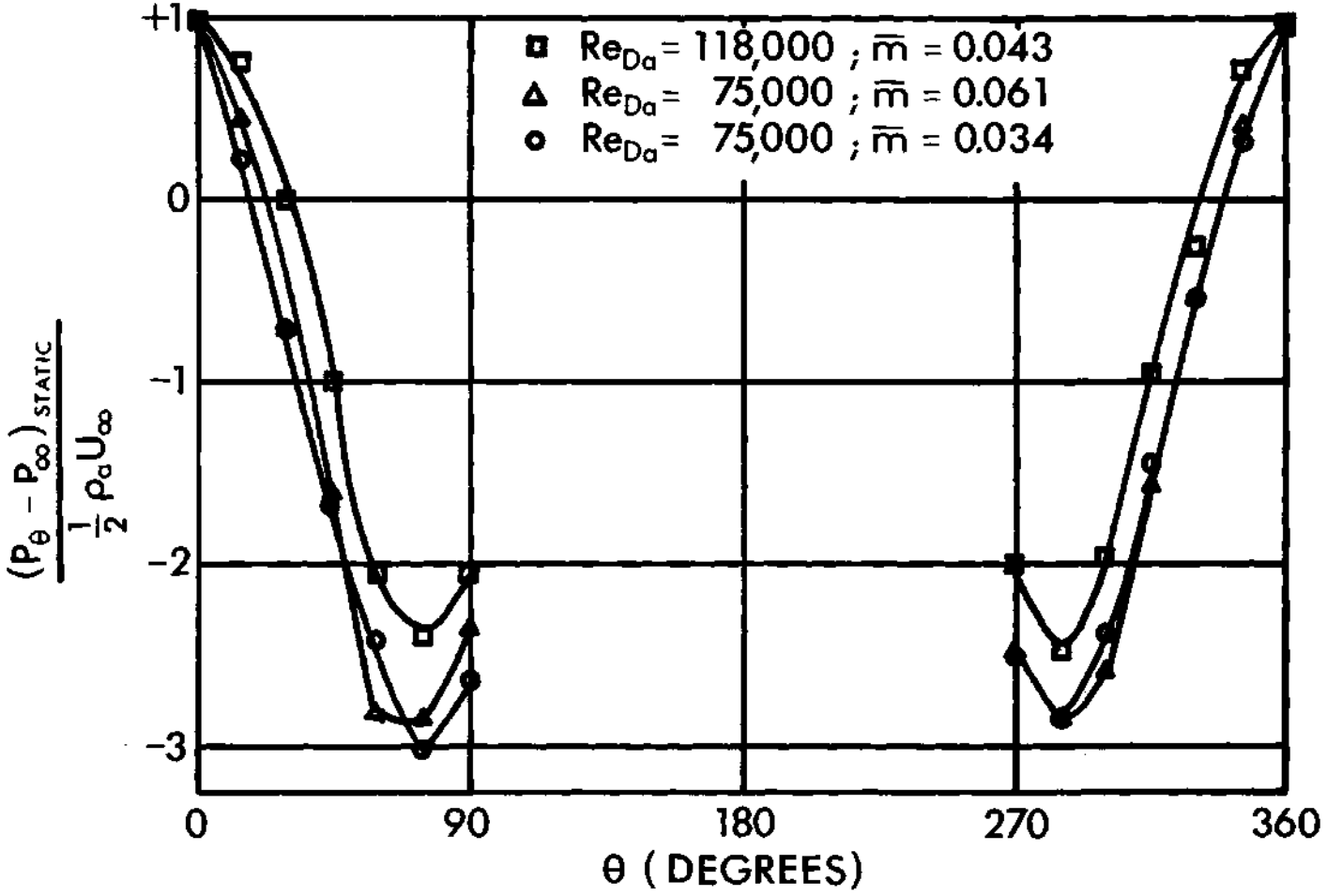

Figure 14. Pressure Distribution Around Plexiglas Cylinder in Two-Component (Air-Water) Flow.

1. Q_s may have been in error by 1.0 per cent due to calibration of the wattmeter.

2. The values of A_s, D, and k_w may have been in error by 1.0 per cent due to measurement of the cylinder and the value used for the thermal conductivity.

3. $(T_s - T_\infty)$ may have been in error by 5.0 per cent due to calibration and fluctuations in the local cylinder surface temperature.

Then performing an error analysis using the above assumed per cent errors, the overall accuracy of the local Nusselt number was ± 7.3 per cent.

Considering the water-air mass flow rate ratio,

$$\bar{m} = \frac{0.1245\left(\rho_w\right)\left(N\right)}{1.328\left(U_\infty\right)\left[\frac{P_{bar.} + \frac{\Delta P}{13.6}}{T_\infty}\right]\left[\frac{1 + \frac{\omega}{7000}}{1 + \frac{\omega}{4360}}\right]}$$

1. N may have been in error by 10 per cent due to lack of repeatability of the average water mass flow rate and the variation in the spray droplet distribution.

2. The air velocity may have been in error by 1.0 per cent.

3. The error of the other terms was considered negligible.

Again, performing an error analysis using the above assumed per cent errors, the overall accuracy of the water-air mass flow rate ratio was ± 11.0 per cent.

Procedure

Heat Transfer Measurements in Two-Component Flow

The experimental procedure used for determining the local Nusselt numbers from the cylinder through the water and air boundary layers for two-component (air-water) flow was as follows:

1. The wind tunnel air wet bulb thermocouple apparatus was filled with water. The thermocouple reference junctions were filled with crushed ice and water.

2. The HTR and the HTR & PC were turned on and calibrated.

3. The three water droplet collection probes were mounted on the horizontal traverse at the test section area, eight-inches upstream from the test cylinder stagnation point.

4. The pitot-static probe was inserted into the wind tunnel, with the probe located at the tunnel centerline and seven-inches upstream from the test cylinder stagnation point. The micromanometer was leveled and adjusted at zero, and then adjusted to the desired velocity pressure.

5. The spray cooling water in the air cooling chamber was started.

6. The fan was started and the damper was adjusted until the desired air velocity in the test section area was obtained.

7. The pitot-static probe was removed.

8. The water spray pump was started and the flow control valve and the pressure regulator valve were adjusted to obtain the desired water spray nozzle pressure.

9. Monitoring was begun of the air dry bulb temperature and the water spray temperature on the HTR.

10. The water spray heaters were connected to the power controller

of the HTR & PC. Monitoring was begun of the water spray temperature, and the air dry and wet bulb temperatures on the HTR & PC. The outputs of the spray cooling water and the water spray heaters were adjusted so the three temperatures were approximately equal.

11. The water spray collection probes were located in the desired position. The water spray collection graduated burettes were emptied.

12. The timer was started and the initial readings of the water levels in the burettes were recorded. At the end of the desired time interval, usually 600 seconds, the final water level readings in the burettes were recorded.

13. Steps 11 and 12 were repeated.

14. When the spray droplet distribution test was completed, the three collection probes were removed from the wind tunnel.

15. The HTR was set to automatic so the air dry bulb temperature, the water spray temperature, and the fourteen cylinder temperatures were recorded on the strip chart.

16. The wattmeter was connected to the appropriate leads on the control board. The external safety jacks were connected across each of the twelve Powerstats to complete each circuit.

17. The Powerstats were turned up and adjusted to obtain an isothermal cylinder surface, usually with a temperature difference between the cylinder surface and the free stream reference temperature of $30^{\circ}F$.

18. The outputs of the spray cooling water and the water spray heaters were adjusted to this new power input into the system.

19. Between five and ten minutes were allowed for the entire system to stabilize.

20. The emfs (mv) of the air dry bulb thermocouple, the water spray thermocouple, and the fourteen cylinder surface thermocouples were determined by the potentiometer and recorded. The wattage to each cartridge heater was determined by the wattmeter and recorded. From the HTR & PC, the wet bulb temperature was determined and recorded.

21. The Powerstats were turned off and the external safety jacks were removed.

22. The water spray pump, the water spray heaters, the spray cooling water, the HTR, the HTR & PC, and the fan were turned off.

Heat Transfer Measurements in One-Component (Air) Flow

The experimental procedure for determining the local Nusselt numbers from the cylinder in one-component (air) flow was similar to the procedure for determining the local Nusselt numbers in two-component (air-water) flow except those procedures involving the introduction and study of the water spray droplets in the system were excluded.

CHAPTER IV

AN ANALYSIS OF TWO-COMPONENT HEAT TRANSFER

An analysis of the liquid film formed on the upstream side of a cylinder exposed to a two-component (gas-liquid) crossflow is presented. The integral forms of the continuity, momentum, and energy equations are used with the goal of determining the local Nusselt number as a function of known parameters. This study includes only the situation with a non-evaporating liquid film on the cylinder surface. Heat transfer across the gas-liquid interface is neglected; therefore, the heat transfer determined by analyzing only the liquid film is an approximate solution for the heat transfer across the liquid film and gas boundary layer. The solutions obtained are applied to a water film formed on the upstream side of a cylinder which is exposed to a two-component (air-water) flow.

The following assumptions are made for the analysis:

1. Steady state flow conditions are considered for the velocity and temperature distributions.

2. The two-dimensional case is considered.

3. All gas and liquid properties (except temperature) are considered constant.

4. The gas and the liquid droplets have the same temperature upstream of the cylinder.

5. Upstream of the cylinder, the liquid droplets are uniformly distributed in the gas stream.

6. The liquid droplets continue in straight paths which are unaffected by the gas flow around the cylinder.

7. The liquid film formed on the upstream side of the cylinder is laminar.

8. The liquid droplets are captured by the liquid film with no "splashing."

9. Body forces are neglected.

10. Evaporation of the liquid film is neglected.

The model considered is shown in Figure 15. A larger view of the control volume abcd is shown in Figure 16.

With these assumptions, solutions will be obtained for the continuity, momentum, and energy equations.

Continuity Equation

Using the integral method, a mass balance on the control volume abcd (Figure 16) is

$$\int_{R}^{R+\delta} \rho_l U_\theta dr\Big|_{\theta} + \dot{m}_l (R + \delta)(\Delta\theta \cos\theta) - \int_{R}^{R+\delta} \rho_l U_\theta dr\Big|_{\theta+\Delta\theta} = 0 \quad . \tag{1}$$

Considering $R \gg \delta$, dividing Equation (1) by $(\rho_l)(\Delta\theta)$, and taking the limit as $\Delta\theta \to 0$ yield

$$\frac{d}{d\theta} \int_{R}^{R+\delta} U_\theta dr = \left(\frac{\dot{m}_l}{\rho_l}\right)\left(R \cos\theta\right) \quad . \tag{2}$$

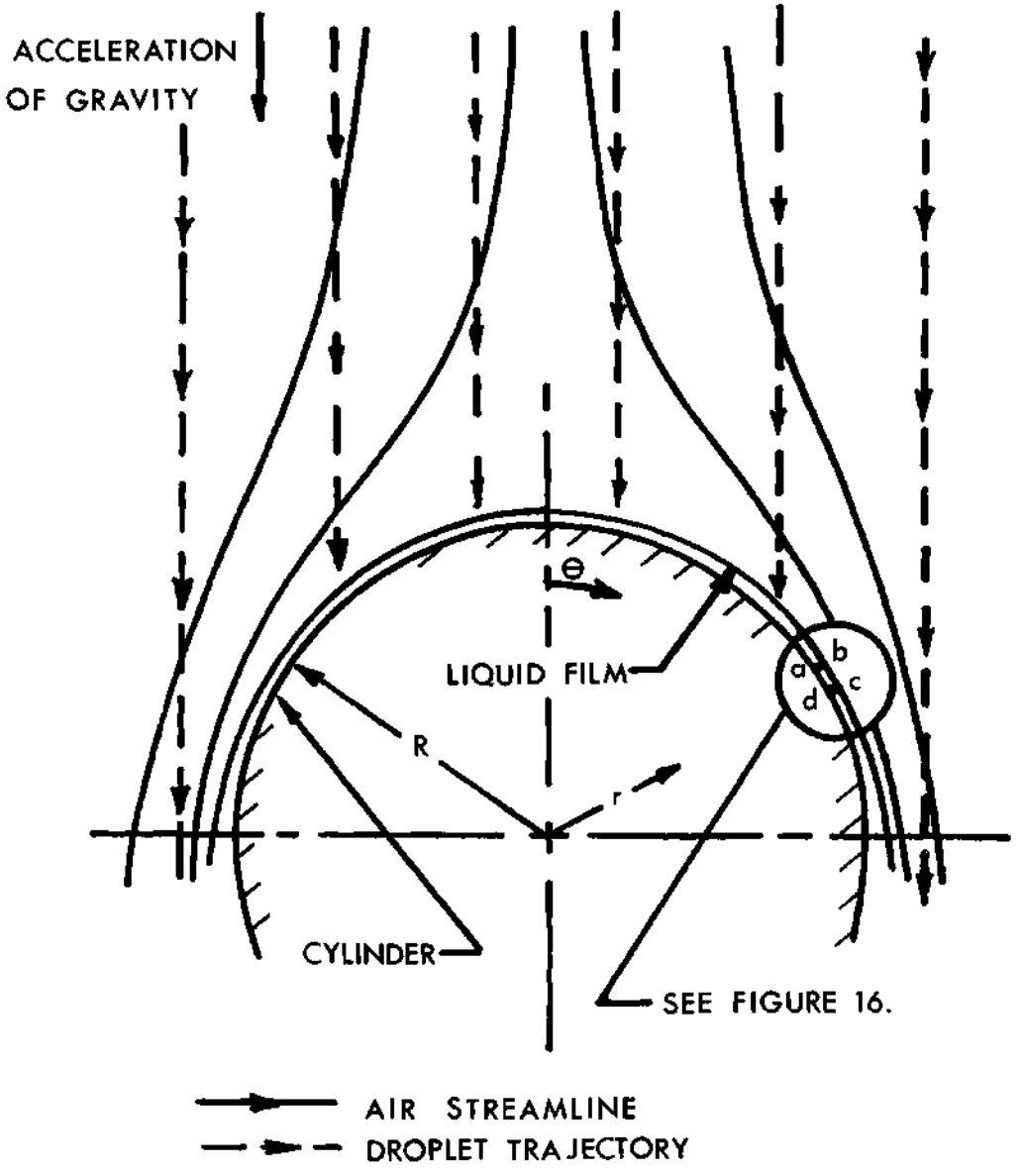

Figure 15. Analytical Model.

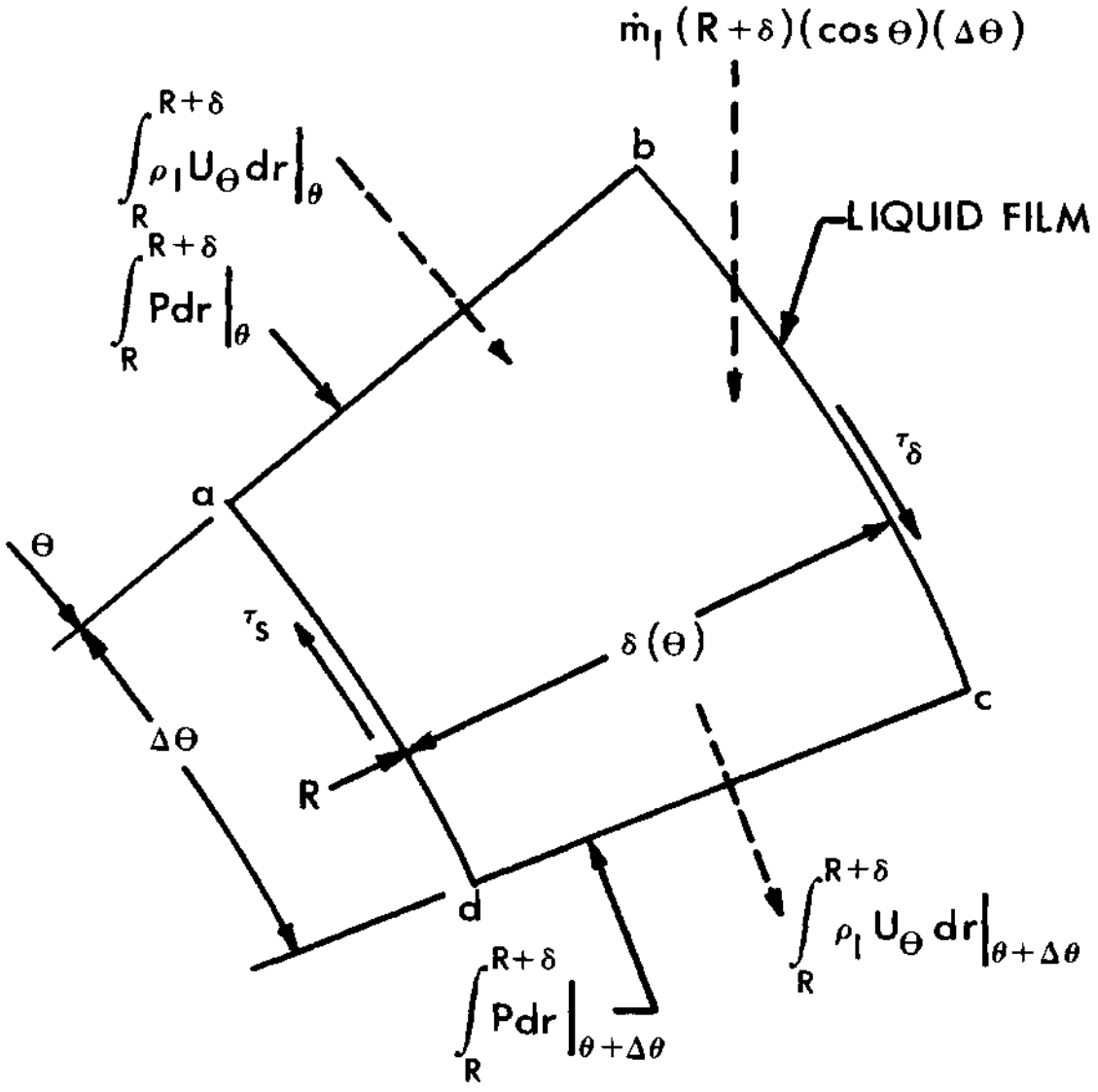

Figure 16. Analytical Model, Control Volume abcd.

Integrating both sides of Equation (2) with respect to θ yields

$$\int_{R}^{R+\delta} U_\theta dr = \left(\frac{\dot{m}_l}{\rho_l}\right)\left(R \sin \theta\right) \quad . \tag{3}$$

A dimensionless linear film velocity profile

$$\frac{U_\theta}{U_\delta} = a + b\,\bar{r} \tag{4}$$

will be assumed, where $\bar{r} = \frac{r-R}{\delta}$, $U_\delta = U_\theta(R+\delta)$, and a and b are coefficients to be determined. The boundary condition for the liquid film at the cylinder surface is $U_\theta(R) = 0$. Then the coefficient a is equal to zero. Therefore, the velocity profile becomes

$$\frac{U_\theta}{U_\delta} = b\,\bar{r} \quad . \tag{5}$$

Substituting Equation (5) into Equation (3), changing the limits of integration, and integrating yield

$$b = 2\left(\frac{\dot{m}_l}{\rho_l}\right)\left(\frac{R \sin \theta}{\delta\, U_\delta}\right) \quad . \tag{6}$$

Then the velocity profile in the liquid film can be written in a dimensionless form

$$\frac{U_\theta}{U_\infty} = 2\left(\frac{\dot{m}_l}{\rho_l}\right)\left(\frac{\sin \theta}{\delta\, U_\infty}\right)\bar{r} \quad , \tag{7}$$

where $\bar{\delta} = \frac{\delta}{R}$ and U_∞ = liquid droplet velocity upstream of the cylinder.

Momentum Equation

The momentum balance in the θ-direction for the control volume abcd is

$$\int_R^{R+\delta} \rho_l U_\theta^2 dr\Big|_{\theta+\Delta\theta} - \left[\int_R^{R+\delta} \rho_l U_\theta^2 dr\Big|_\theta + \dot{m}_l(R+\delta)(U_\infty \sin\theta)(\Delta\theta \cos\theta)\right] \tag{8}$$

$$= -\tau_s(R\Delta\theta) + \tau_\delta(R+\delta)(\Delta\theta) + \int_R^{R+\delta} P\, dr\Big|_\theta - \int_R^{R+\delta} P\, dr\Big|_{\theta+\Delta\theta} .$$

Rearranging Equation (8), considering $R \gg \delta$, dividing by $(R\Delta\theta)$, and taking the limit as $\Delta\theta \to 0$, yield

$$\frac{1}{R}\frac{d}{d\theta}\int_R^{R+\delta} \rho_l U_\theta^2\, dr + (\tau_s - \tau_\delta) + \frac{1}{R}\frac{d}{d\theta}\int_R^{R+\delta} P\, dr - \dot{m}_l U_\infty(\cos\theta \sin\theta) \tag{9}$$

$$= 0 .$$

The following assumptions are made:

1. The liquid film momentum in the θ-direction is neglected.

2. Pressure gradients in the liquid film are neglected.

3. The gas shear force on the liquid film at the gas-liquid interface is neglected.

An order of magnitude analysis indicated that the momentum in the θ-direction can be neglected, especially at low liquid-gas mass flow rate ratios.

Then Equation (9) becomes

$$\tau_s - \dot{m}_1 U_\infty(\cos\theta \sin\theta) = 0 \quad . \tag{10}$$

The shear stress on the liquid film at the cylinder surface is

$$\tau_s = \mu_1 \frac{\partial U_\theta}{\partial r}\Big|_{r=R}$$

where $U_\theta = U_\delta \; b\,\bar{r}$, and $\partial r = \delta\,\partial\,\bar{r}$.

Rewriting Equation (10) yields

$$\mu_1 \left(\frac{b}{\delta}\right)(U_\delta) = \dot{m}_1 U_\infty (\cos\theta \sin\theta) \quad . \tag{11}$$

Substituting the value of b from Equation (6) into Equation (11) and rearranging yield

$$\frac{\delta^2}{R^2} = \bar{\delta}^2 = \frac{4}{(Re_{D1})(\cos\theta)} \quad . \tag{12}$$

Equation (12) is a dimensionless expression for the liquid film thickness on the upstream side of the cylinder in the laminar region, expressed in terms of the liquid free stream Reynolds number and the angle from the stagnation point. The expression for the liquid film thickness breaks down near 90 degrees, for at 90 degrees the liquid film thickness becomes undefined.

Energy Equation

The energy balance on the control volume abcd is

$$\int_{R}^{R+\delta} \rho_l U_\theta H_{l\theta}\, dr\Big|_\theta + \dot{m}_l H_{l\infty} (R + \delta)(\Delta\theta \cos\theta)$$

$$+ (-k_l)(R\Delta\theta) \frac{\partial T_\theta}{\partial r}\Big|_{r=R} - \int_{R}^{R+\delta} \rho_l U_\theta H_{l\theta}\, dr\Big|_{\theta+\Delta\theta} = 0 \quad , \tag{13}$$

where

1. Convective heat transfer across the gas-liquid interface is neglected.

2. Conduction heat transfer in the θ-direction in the liquid film is neglected.

3. Evaporation heat transfer from the liquid film to the droplet laden air stream is neglected.

Rearranging Equation (13), considering $R \gg \delta$, dividing by $\Delta\theta$, and taking the limit as $\Delta\theta \to 0$ yield

$$\frac{d}{d\theta} \int_{R}^{R+\delta} \rho_l U_\theta H_{l\theta}\, dr - \dot{m}_l H_{l\infty} (R \cos\theta) = -k_l R \frac{\partial T_\theta}{\partial r}\Big|_{r=R} \quad . \tag{14}$$

Now using the gas and liquid droplet temperature as a reference temperature for determining enthalpies and assuming $H = c_p(T-T_{ref}) = c_p(T-T_\infty)$ yield

$$H_{l\theta} = c_{pl}(T_\theta - T_\infty) \quad .$$

Therefore, Equation (14) can be rewritten

$$\frac{d}{d\theta}\int_{R}^{R+\delta} \rho_l U_\theta c_{pl}(T_\theta - T_\infty)\, dr = - k_l R \frac{\partial T_\theta}{\partial r}\bigg|_{r=R} \quad . \tag{15}$$

Now define $\phi_T = (T_\theta - T_\infty)/(T_s - T_\infty)$ and assume a linear temperature profile in the liquid film of the form

$$T_\theta = c + d\,\bar{r} \tag{16}$$

where c and d are coefficients to be determined. The temperature boundary conditions on the liquid film are

1. $T_\theta = T_s$ at $\bar{r} = 0$; $\quad c = T_s$

2. $T_\theta = T_\delta$ at $\bar{r} = 1$; $\quad d = T_\delta - T_s$.

Rearranging Equation (15) yields

$$\frac{d}{d\theta}\int_{0}^{1}\left(\frac{U_\theta}{U_\infty}\right) \phi_T\, \bar{\delta}\, d\,\bar{r} = \frac{-2}{\left(Re_{Dl}\right)\left(Pr_l\right)\left(\bar{\delta}\right)} \left(\frac{\partial \phi_T}{\partial \bar{r}}\right)\bigg|_{\bar{r}=0} \quad . \tag{17}$$

Now

$$\phi_T = 1 - \bar{r}\left(\frac{\Psi_\delta}{\Psi_\infty}\right) \tag{18}$$

where $\Psi = T_s - T$.

Substituting U_θ/U_∞ from Equation (7) and ϕ_T from Equation (18) into Equation (17) yields

$$\frac{d}{d\theta}\int_0^1 2\left(\frac{\dot{m}_l}{\rho_l}\right)\left(\frac{\sin\theta}{U_\infty}\right)(\bar{r})\left(1-\bar{r}\,\frac{\Psi_\delta}{\Psi_\infty}\right)\,d\bar{r} = \frac{-2}{\left(Re_{Dl}\right)\left(Pr_l\right)(\bar{\delta})}\left(\frac{\partial\phi_T}{\partial\,\bar{r}}\right)\Bigg|_{\bar{r}=0} \quad .(19)$$

Integrating the left side and differentiating the right side of Equation (19) yield, after arranging into dimensionless form

$$\left(\frac{\bar{m}}{\bar{\rho}}\right)\frac{d}{d\theta}\left[\left(\frac{1}{2}-\frac{1}{3}\,\frac{\Psi_\delta}{\Psi_\infty}\right)\sin\theta\right] = \frac{1}{\left(Re_{Dl}\right)\left(Pr_l\right)(\bar{\delta})}\left(\frac{\Psi_\delta}{\Psi_\infty}\right), \qquad (20)$$

where $\bar{m} = \dot{m}_l/\dot{m}_g$ and $\bar{\rho} = \rho_l/\rho_g$.

Differentiating the left side of Equation (20) and rearranging yield the differential equation

$$\frac{d}{d\theta}\left(\frac{\Psi_\delta}{\Psi_\infty}\right) + \left[\cot\theta + 3\left(\frac{\bar{\rho}}{\bar{m}}\right)\frac{1}{\left(Re_{Dl}\right)\left(Pr_l\right)(\sin\theta)(\bar{\delta})}\right]\left(\frac{\Psi_\delta}{\Psi_\infty}\right) - \frac{3}{2}\cot\theta = 0 \quad . \qquad (21)$$

The first term of Equation (21) will be assumed negligible compared to the other terms of the equation. By disregarding the first term of Equation (21), the resulting solution is limited to a range of θ from 0 to approximately 70 degrees from the stagnation point. Above this limit of 70 degrees, the differential term becomes of the same order of magnitude as the last term of Equation (21), and therefore it cannot be neglected. By rearranging Equation (21), the temperature distribution becomes

$$\frac{\Psi_\delta}{\Psi_\infty} = \frac{1.5 \cos\theta}{\left[\cos\theta + 3\left(\frac{\bar{\rho}}{\bar{m}}\right)\frac{1}{\left(Re_{D1}\right)\left(Pr_1\right)\left(\bar{\delta}\right)}\right]} \quad . \tag{22}$$

The local heat transfer coefficient from the cylinder surface to the two-component (gas-liquid) stream is given by

$$h\Big|_\theta = \frac{-k_1}{(T_s - T_\infty)}\left(\frac{\partial T_\theta}{\delta\, \partial \bar{r}}\right)\Bigg|_{\bar{r}=0} \quad . \tag{23}$$

Rewritten, Equation (23) becomes

$$h\Big|_\theta = \left(\frac{k_1}{\delta}\right)\left(\frac{\Psi_\delta}{\Psi_\infty}\right)\Bigg|_\theta \quad . \tag{24}$$

By substituting the value of Ψ_δ/Ψ_∞ from Equation (22) into Equation (24), and the value of δ from Equation (12), the local heat transfer coefficient becomes

$$h\Big|_\theta = \frac{1.5\, k_1 \sqrt{Re_{D1}}\,(\cos\theta)^{3/2}}{D\left[\cos\theta + 3\left(\frac{\bar{\rho}}{\bar{m}}\right)\frac{1}{\left(Re_{D1}\right)\left(Pr_1\right)\left(\bar{\delta}\right)}\right]} \quad . \tag{25}$$

Substituting the value of $\bar{\delta}$ from Equation (12) into Equation (25) and then rewriting Equation (25) in terms of the gas free stream Reynolds number yield

$$h\Big|_{\theta} = \frac{1.5\, k_1 \sqrt{Re_{Dg}}\,(\cos\theta)^{3/2}}{D\sqrt{\bar{\nu}}\left[\cos\theta + 1.5\left(\frac{\bar{\rho}}{\bar{m}}\right)\frac{\sqrt{\cos\theta}}{Pr_1}\sqrt{\frac{\bar{\nu}}{Re_{Dg}}}\right]} \tag{26}$$

where $\bar{\nu} = \nu_1/\nu_g$. Now, expressing Equation (26) in dimensionless form and rearranging (cos θ) yield

$$\frac{hD}{k_1}\Big|_{\theta} = Nu_{D1}\Big|_{\theta} = \frac{1.5\sqrt{Re_{Dg}\cos\theta}}{\sqrt{\bar{\nu}}\left[1 + 1.5\left(\frac{\bar{\rho}}{\bar{m}}\right)\left(\frac{1}{Pr_1}\right)\sqrt{\frac{\bar{\nu}}{Re_{Dg}\cos\theta}}\right]}. \tag{27}$$

Equation (27) is the local Nusselt number from the cylinder across the liquid and gas boundary layers to the liquid droplet laden gas stream. The liquid droplet velocity is assumed equal to the gas velocity far upstream of the cylinder. The gas properties are evaluated at the free stream reference temperature. The liquid properties are evaluated at the average temperature between the free stream reference temperature and the cylinder surface temperature, except the liquid kinematic viscosity which is evaluated at the cylinder surface temperature.

The local Nusselt number determined by Equation (27) is compared with experimental results for the case of liquid water droplets borne by an air stream. The results are shown in Figures 27, 28, and 29.

CHAPTER V

PRESENTATION AND DISCUSSION OF RESULTS

Introduction

Measurements were made to determine the local and overall Nusselt numbers for a circular cylinder exposed to a saturated air stream with entrained water droplets. These results are compared with data obtained by previous investigators. The heat transfer results from this investigation for two-component flow are expressed in terms of the Nusselt number, instead of the heat transfer coefficient. For comparison, it was necessary to convert data reported by previous investigators from heat transfer coefficients to Nusselt numbers. Also, the experimentally determined local Nusselt numbers are compared with the analytical Nusselt numbers obtained in Chapter IV.

Since there are many variables which could influence the heat transfer characteristics and which have not been thoroughly investigated, it is difficult to make a conclusive comparison of previous data with the data of this investigation. The variables include the water droplet diameter, the water droplet velocity and its relationship to the air velocity, the air velocity, the spray droplet distribution and the water mass flow rate, the cylinder temperature, the water spray and air temperatures, and the orientation of the cylinder to the two-component flow.

This investigation was limited to determining the effects of the air free stream Reynolds number and the water-air mass flow rate ratio on

the heat transfer characteristics. Cylinder surface and water spray temperatures were chosen so only sensible heating of the film was significant.

Experimental Results

Heat Transfer in One-Component (Air) Flow

In one-component (air) flow (Tables 1 through 4), the overall Nusselt numbers for the cylinder were higher for the Reynolds numbers of 30,000, 75,000, and 118,000 (Figure 17) when compared with Hilpert (11). This increase could have been caused by a high turbulence intensity in the test section area. For all three Reynolds numbers, the heat transfer was not symmetric with the stagnation point. Two Nusselt number minima were experienced on one side of the cylinder while only one Nusselt number minimum existed on the other side. Flow separation occurred at 120 degrees on the side with two minima and at 90 degrees on the side with only one minimum.

Heat Transfer in Two-Component (Air-Water) Flow

The experimental results of heat transfer from an isothermal cylinder exposed to a saturated air stream with entrained water droplets are presented in tabular form in Tables 1 and 5 through 23. A representative part of these data is plotted in graphical form in Figures 18 through 29.

The addition of water droplets to the air stream does increase the local Nusselt number around the cylinder (Figures 18, 19, and 20). In all cases, the maximum local Nusselt number was experienced at the cylinder stagnation point. The local Nusselt number decreased almost linearly

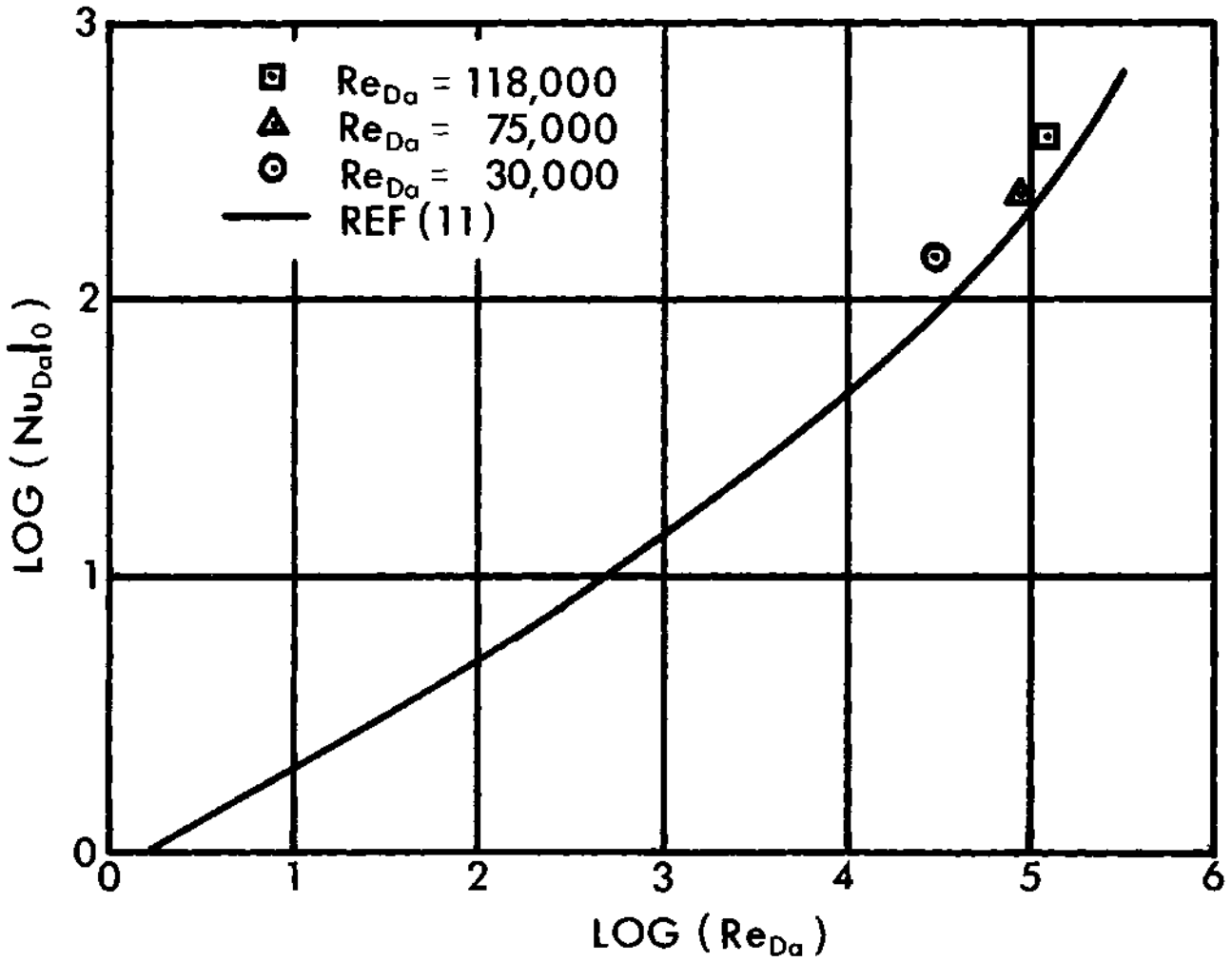

Figure 17. Overall Nusselt Number versus Reynolds Number for One-Component (Air) Flow.

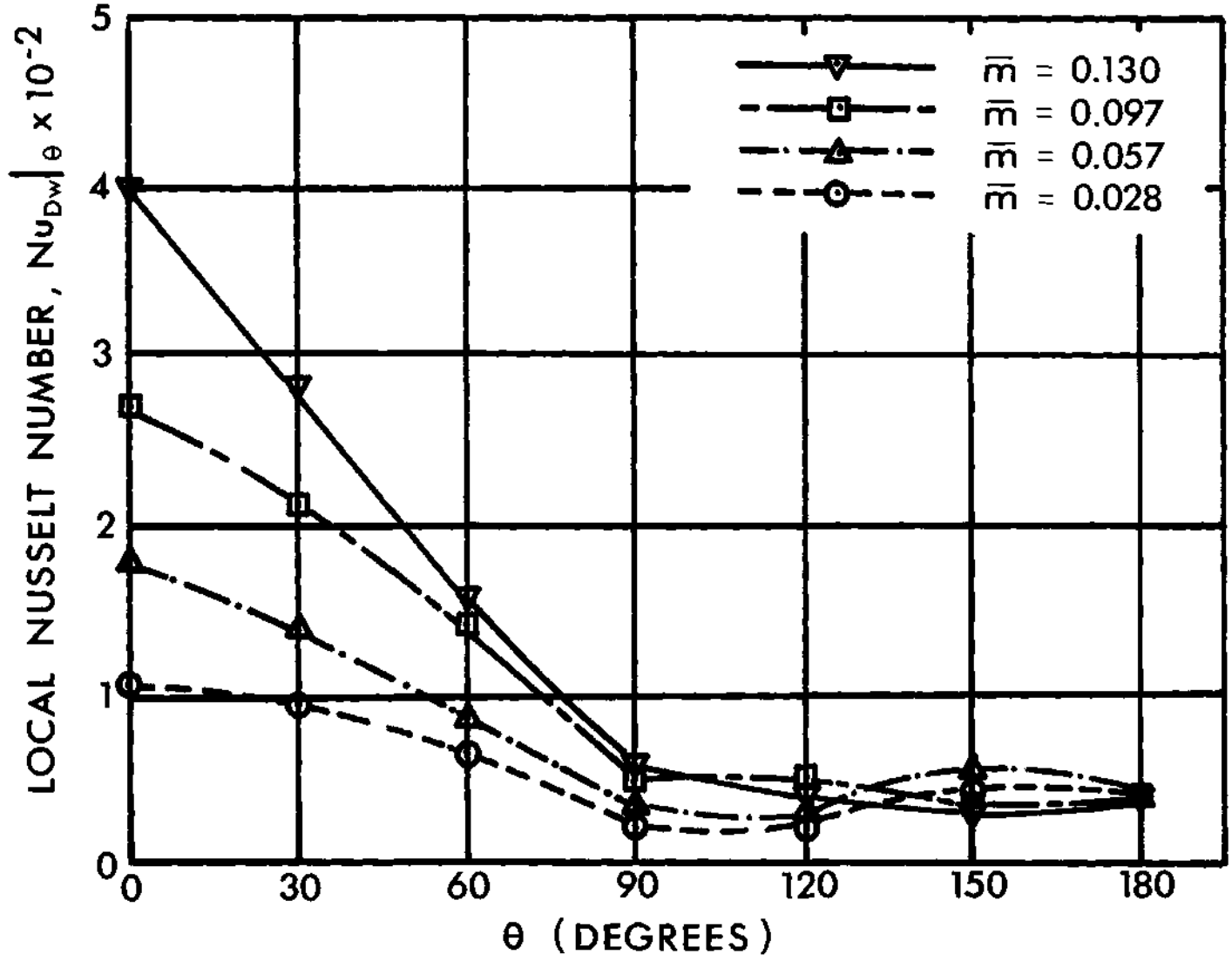

Figure 18. Experimental Local Nusselt Number for Re = 30,000 in Two-Component Flow.

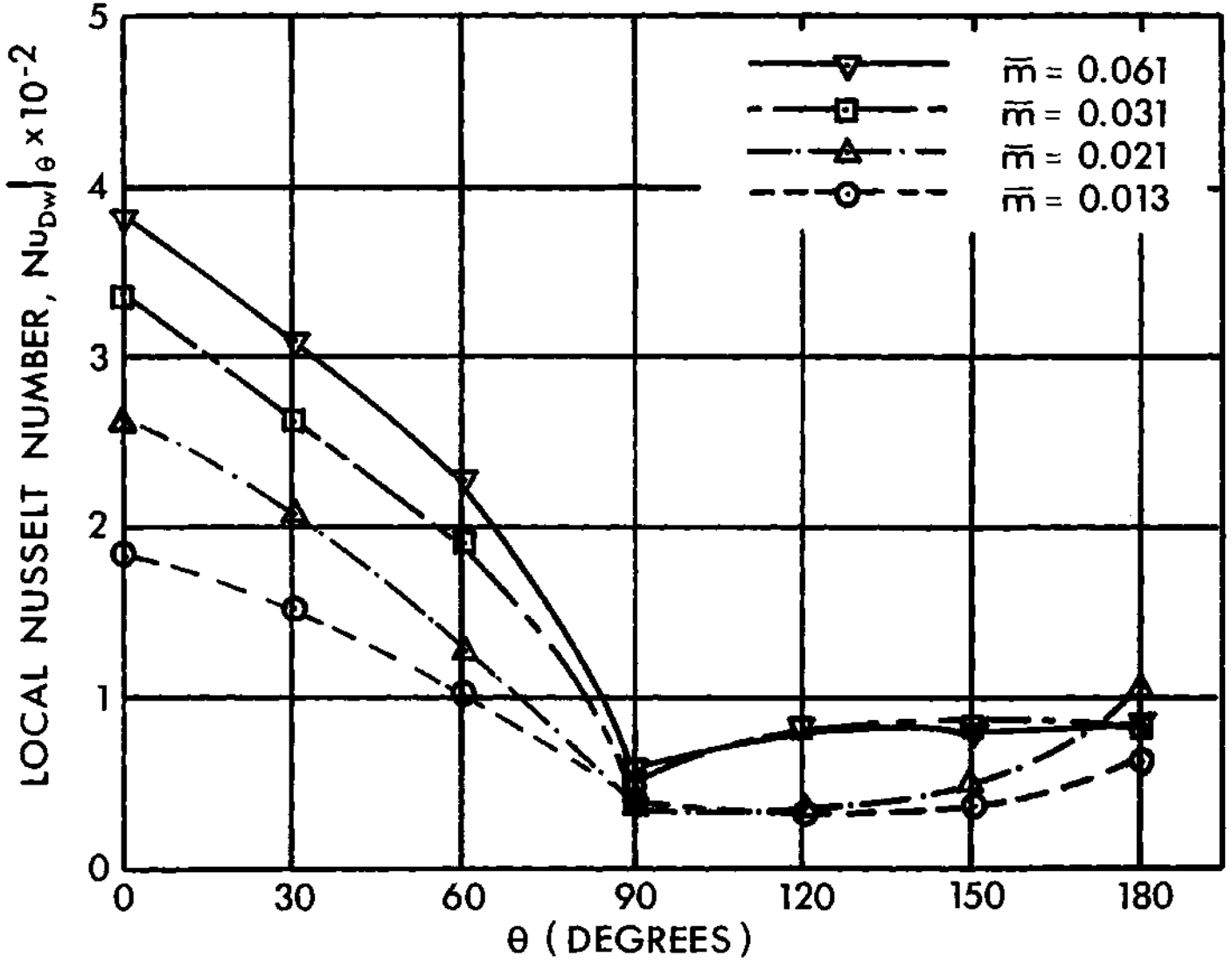

Figure 19. Experimental Local Nusselt Number for Re = 75,000 in Two-Component Flow.

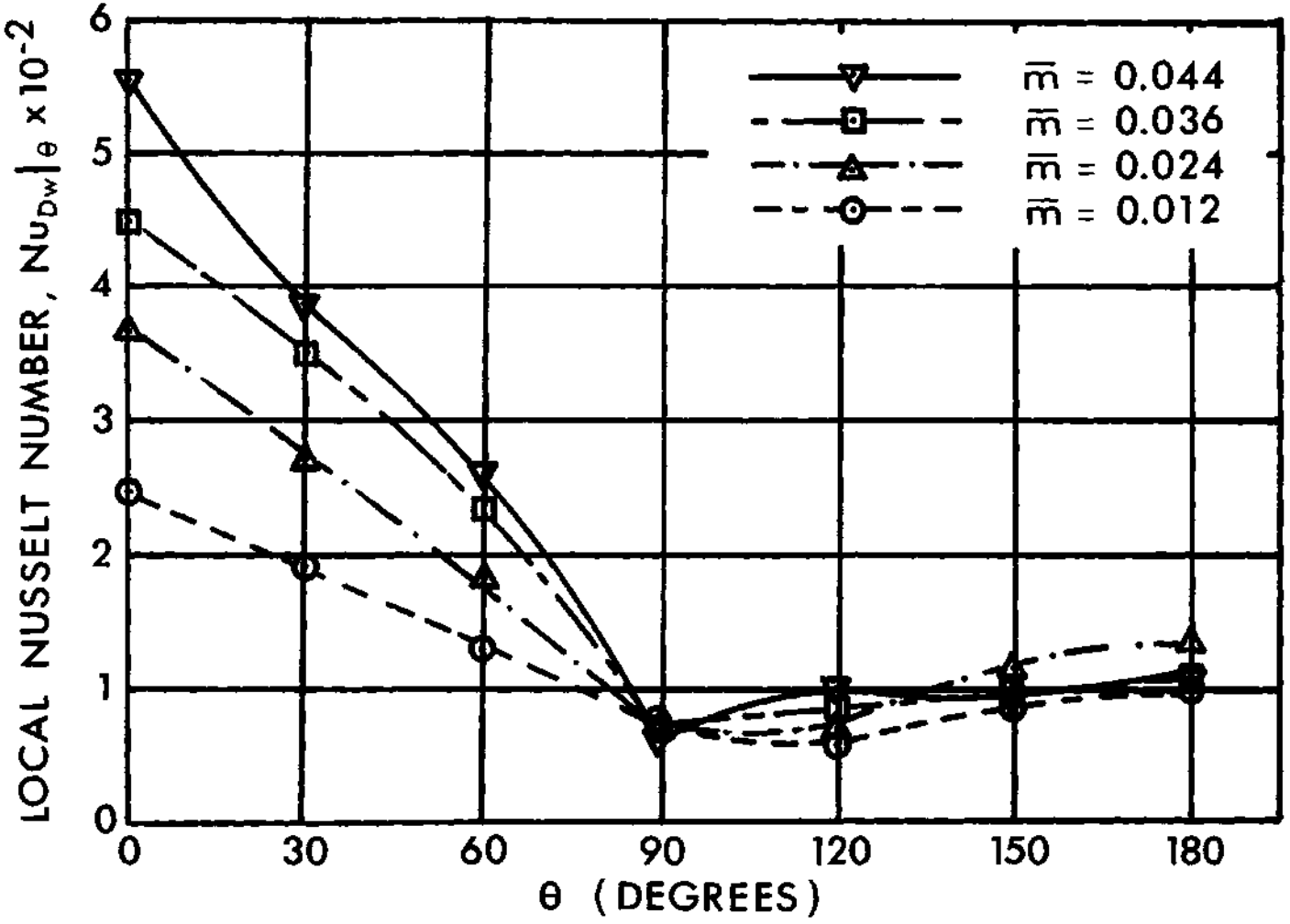

Figure 20. Experimental Local Nusselt Number for Re = 118,000 in Two-Component Flow.

with angular position from the stagnation point to 90 degrees where the local Nusselt number was almost constant with respect to a given Reynolds number. For a constant Reynolds number, the local Nusselt number on the upstream side of the cylinder increased with an increase in water-air mass flow rate ratio. The heat transfer on the downstream side of the cylinder remained nearly independent of the water-air mass flow rate ratio for a given Reynolds number. The heat transfer from the downstream side of the cylinder contributed from 15 to 30 per cent of the total cylinder heat transfer, with the per cent decreasing as the water-air mass flow rate ratio increased. A maximum local Nusselt number of 557 was recorded at the stagnation point for a Reynolds number of 118,000 and a water-air mass flow rate ratio of 0.044. A minimum stagnation point Nusselt number of 108 was experienced for a Reynolds number of 30,000 and a water-air mass flow rate ratio of 0.028. The stagnation point heat transfer in two-component flow was from 11 to 58 times greater than in one-component (air) flow.

The overall Nusselt number for the cylinder increased with the addition of the water droplets to the air stream (Figures 21, 22, and 23). The overall heat transfer in two-component flow was from 7 to 23 times greater than in one-component (air) flow. The overall Nusselt numbers in two-component flow were 7 to 19 per cent of the overall Nusselt numbers obtained by McAdams (12) for a cylinder submerged in water crossflow. At a Reynolds number of 30,000, the overall Nusselt number increased linearly with an increase in water-air mass flow rate ratio (Figure 21). A cross-plot of Figure 21 shows that the overall Nusselt number may vary linearly with an increase in Reynolds number for a constant water-air mass flow

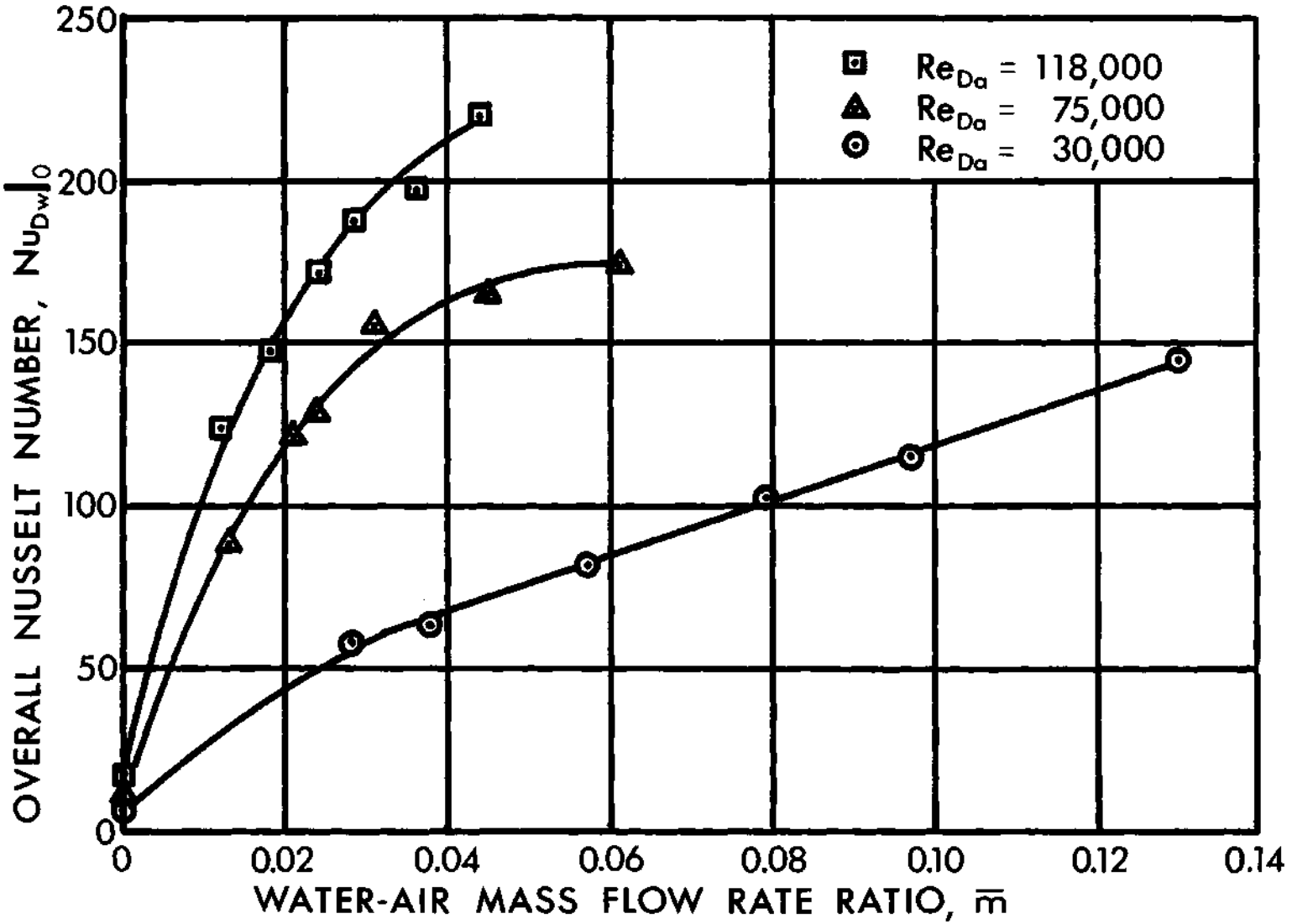

Figure 21. Overall Nusselt Number versus Water-Air Mass Flow Rate Ratio for Two-Component Flow.

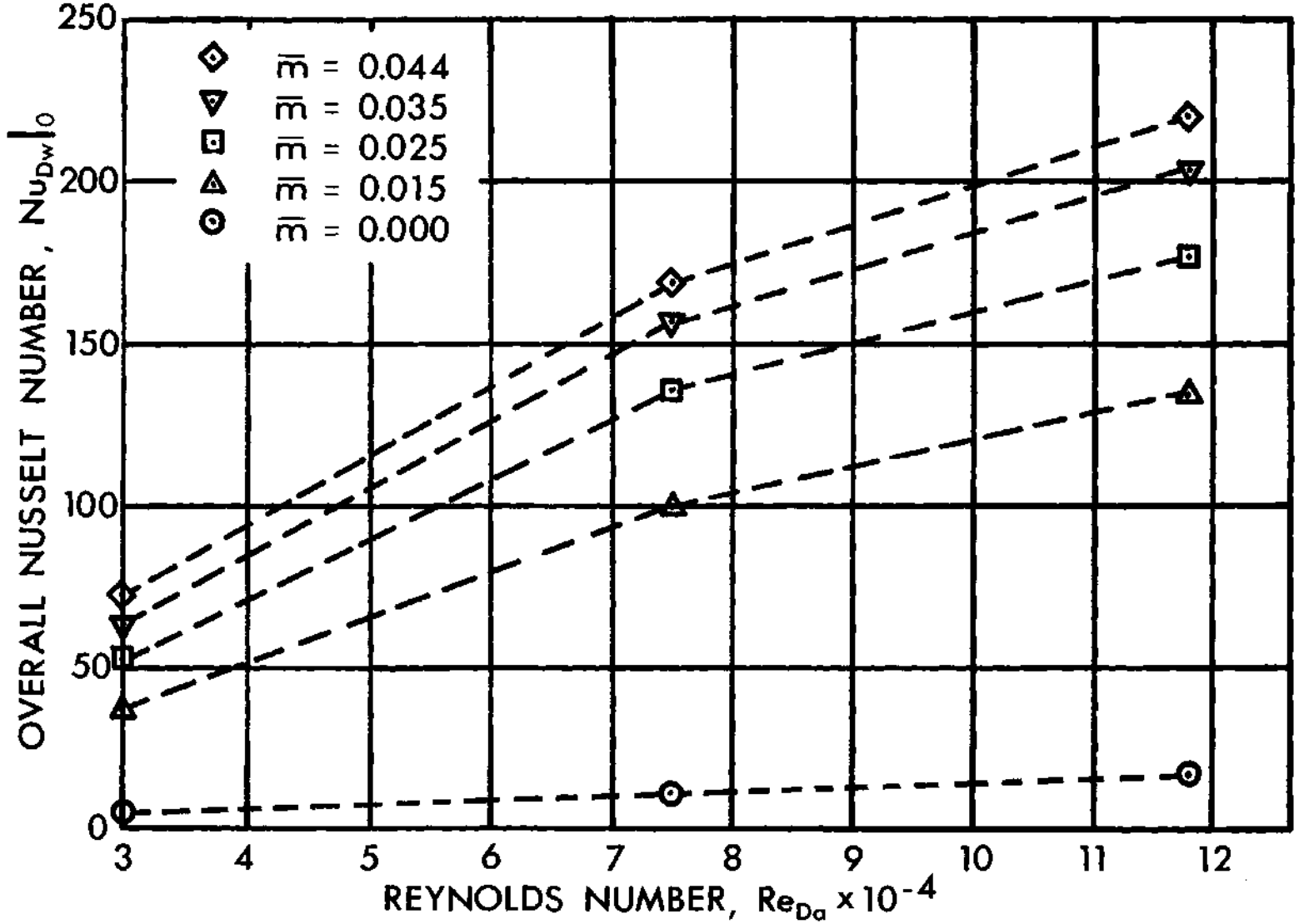

Figure 22. Overall Nusselt Number versus Reynolds Number for Two-Component Flow.

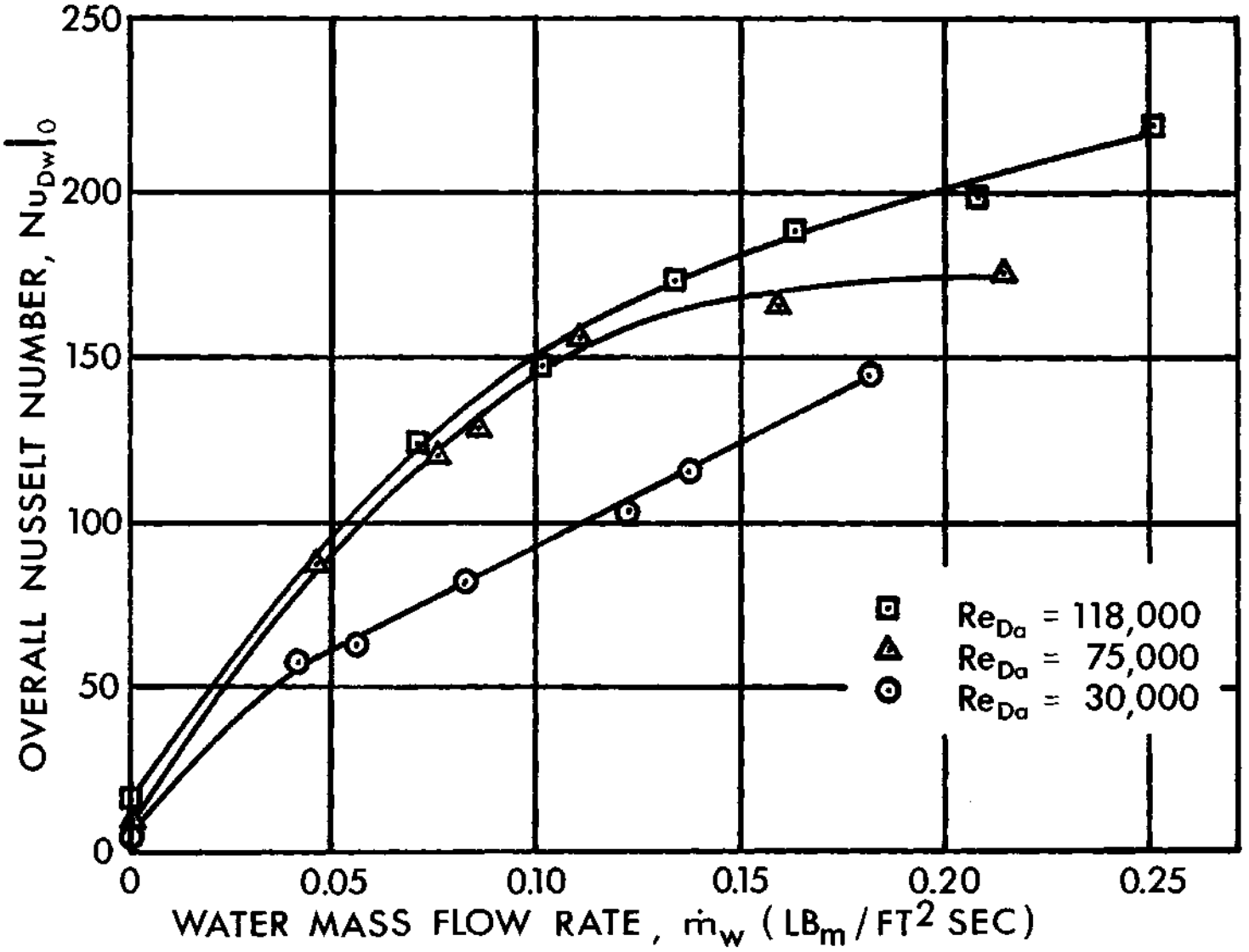

Figure 23. Overall Nusselt Number versus Water Mass Flow Rate for Two-Component Flow.

rate ratio. Due to the degree of uncertainty of the overall Nusselt numbers for interim Reynolds numbers between actual measurements, dashed lines were used in Figure 22.

The overall Nusselt number was plotted against the water mass flow rate (Figure 23). A linear increase in overall Nusselt number existed for the Reynolds number of 30,000. The overall Nusselt number for the Reynolds number of 75,000 was only ten per cent lower than the Nusselt number for the Reynolds number of 118,000 for the water mass flow rates from 0.05 to 0.12 lbm/ft^2-sec.

At the Reynolds number of 75,000, a test was made to determine the effects that the temperature difference between the cylinder surface and the free stream reference temperature had on the local and overall Nusselt numbers (Table 23). A free stream reference temperature of $80^{\circ}F$ with cylinder surface temperatures of 101, 112, and $123^{\circ}F$ were used. The local Nusselt numbers on the upstream side of the cylinder increased with each increase in temperature difference. The overall Nusselt number increased eight per cent with each increase in temperature difference. This increase in heat transfer could have been due to errors within the system and/or an increase in film evaporation and convective heat transfer.

Good wetting characteristics were experienced with a liquid water film covering the entire cylinder surface for the heat transfer tests. Since the test cylinder was mounted horizontally, water running onto the test section from other sections of the cylinder was not experienced. Also, the liquid film remained on the cylinder and a high accumulation of water was experienced in the area 180 degrees from the stagnation point. By using a Strobotac light, splashing and waves were observed in the

liquid film on the upstream side of the cylinder for the Reynolds number of 118,000.

To obtain reliable heat transfer data it was necessary to maintain an isothermal cylinder surface. During the tests, the local cylinder surface temperatures recorded at the heater centerlines varied from ± 0.3 to ± 0.5°F from the average cylinder surface temperature. The two thermocouples, each located 1/4-inch off center of a main centerline thermocouple, indicated that the temperature increased from 1 to 3°F in the circumferential direction, thus questioning the isothermal characteristics of the cylinder surface. The heat transfer from the cylinder was reasonably symmetric with the centerline except for one heater located 30 degrees from the stagnation point. In some cases, the wattage of this heater was equal to or higher than the wattage of the stagnation point heater. The cylinder was rotated 30 degrees and the wattage loads became reasonably symmetric. Other variations in nonsymmetric wattage output by the heaters could have been due to unsymmetric spray distribution.

The effect of the water droplet diameter on the heat transfer was not studied; but, from Figure 12, it can be seen that the mass median water droplet diameter could have varied from 120 to 300 microns. A reliable and easy method to determine the average water spray droplet velocity was not obtained.

The local Nusselt numbers obtained in this investigation were compared with the results of Takahara (3) and Smith (4) for Reynolds numbers of 110,000 and 120,000 and with Takahara at a Reynolds number of 77,000 (Figures 24 and 25). The data reported by Acrivos (1) and Hoelscher (2) were not compared. At both Reynolds numbers, Takahara experienced much

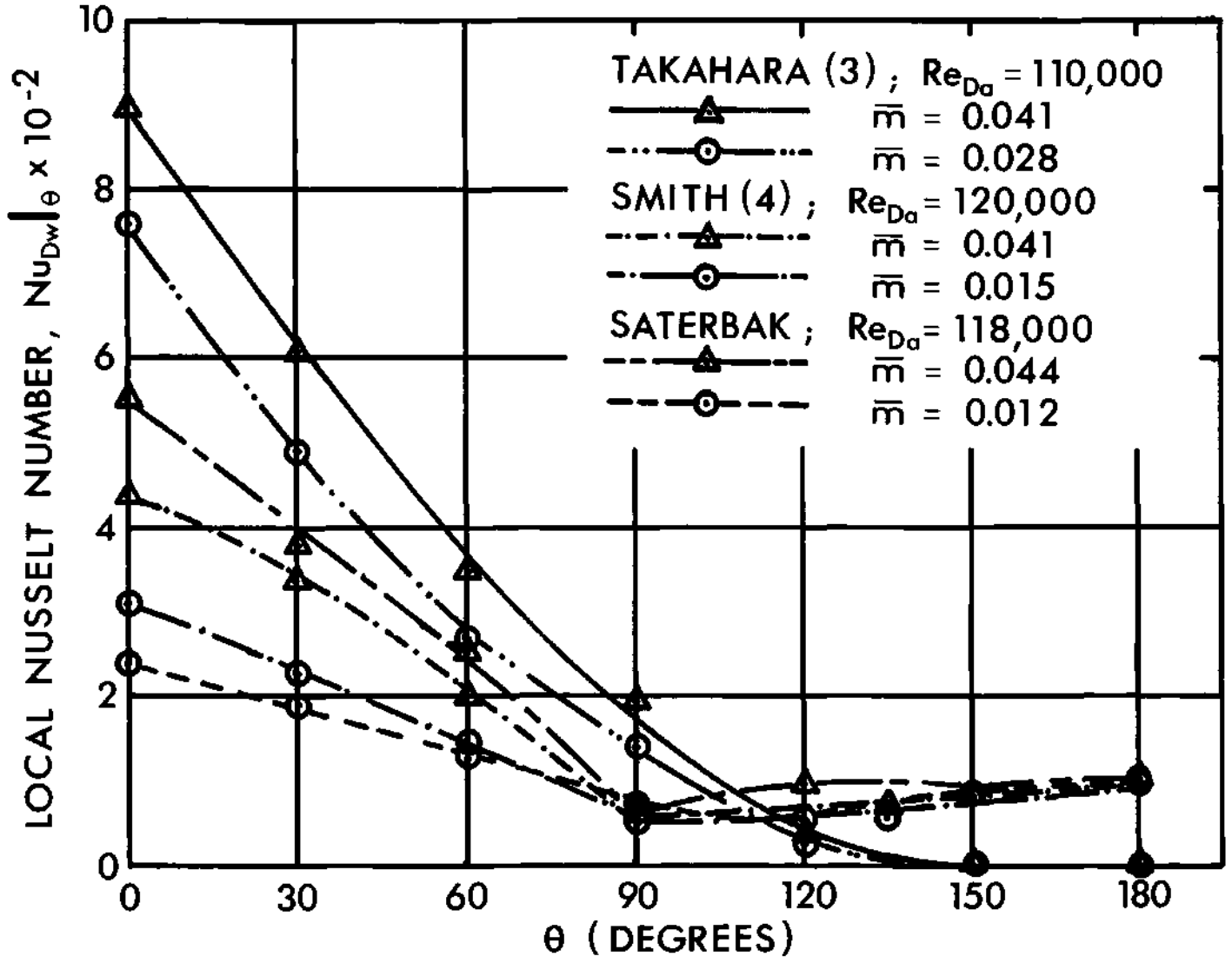

Figure 24. Comparison of Experimental Local Nusselt Number for Two-Component Flow.

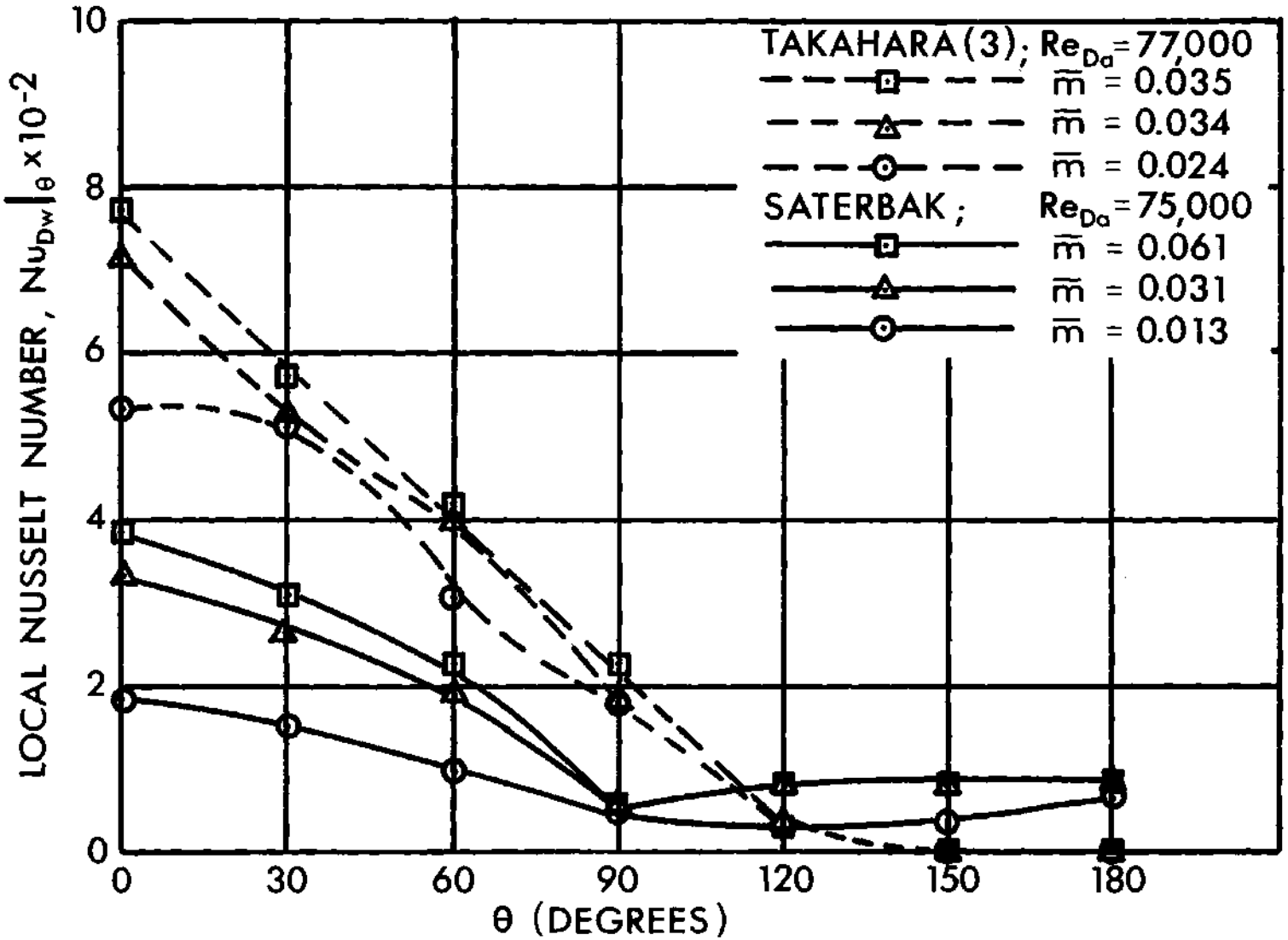

Figure 25. Comparison of Experimental Local Nusselt Number for Two-Component Flow.

higher stagnation point Nusselt numbers than results published by Smith or obtained in this investigation. Also, Takahara reported insignificant heat transfer on the downstream side of the cylinder for the Reynolds numbers of 77,000 and 110,000. Smith and this investigator obtained results indicating the heat transfer on the downstream side of the cylinder accounted for 15 to 30 per cent of the total heat transfer. The local Nusselt numbers obtained by Smith and this investigator were consistent with the water-air mass flow rate ratios for the Reynolds number of 118,000.

The overall Nusselt numbers obtained by Takahara (3), Smith (4), and this investigator were compared in Figure 26. Even though Takahara reported much higher stagnation point Nusselt numbers, the overall Nusselt numbers were considerably lower for both Reynolds numbers. The overall Nusselt numbers reported by Smith and obtained in this investigation compared very favorably for the Reynolds number of 118,000.

Analytical Results

The analytically determined local Nusselt numbers are compared with the experimental results for the air Reynolds numbers of 30,000, 75,000, and 118,000. A representative part of these data is presented in Figures 27, 28, and 29.

In the case of considering only sensible heating of the liquid film with no evaporation, an upper limit exists when the droplets, upon impingement on the cylinder, immediately heat up to the cylinder surface temperature. The analytical study presented in this investigation was a first approximation to this upper limit in determining the local Nusselt

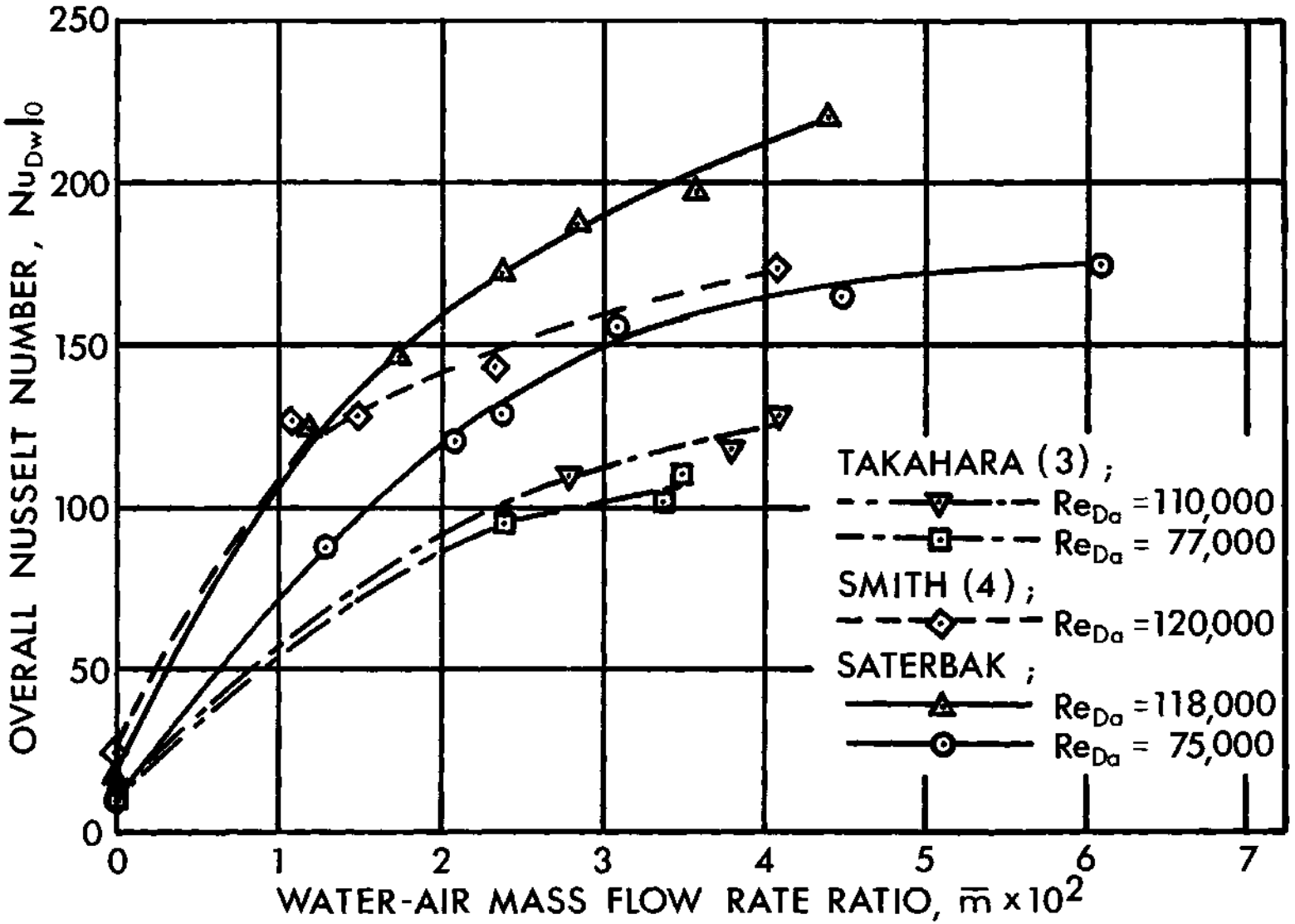

Figure 26. Comparison of Overall Nusselt Number versus Water-Air Mass Flow Rate Ratio for Two-Component Flow.

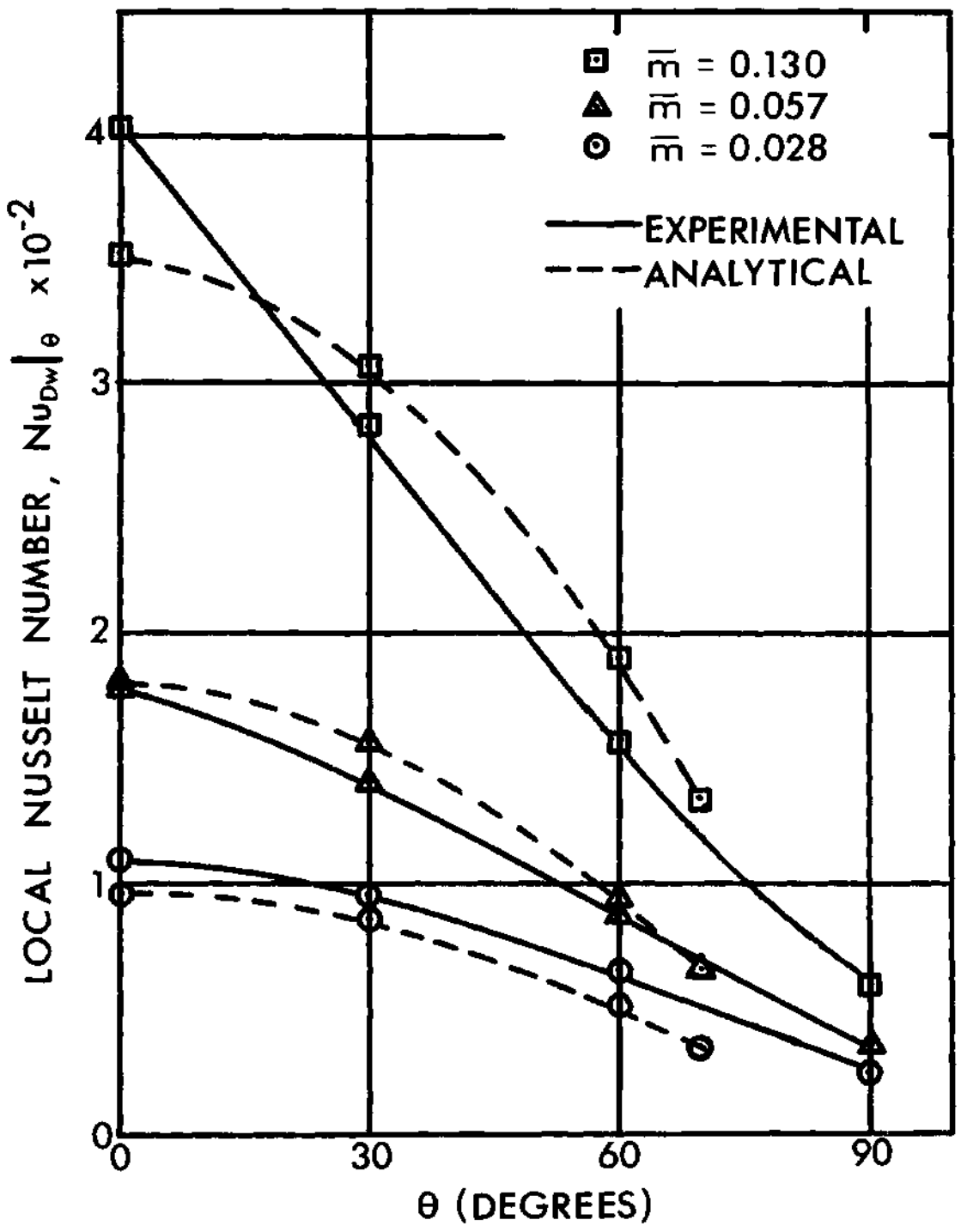

Figure 27. Comparison of Experimental and Analytical Local Nusselt Numbers for Re = 30,000 in Two-Component Flow.

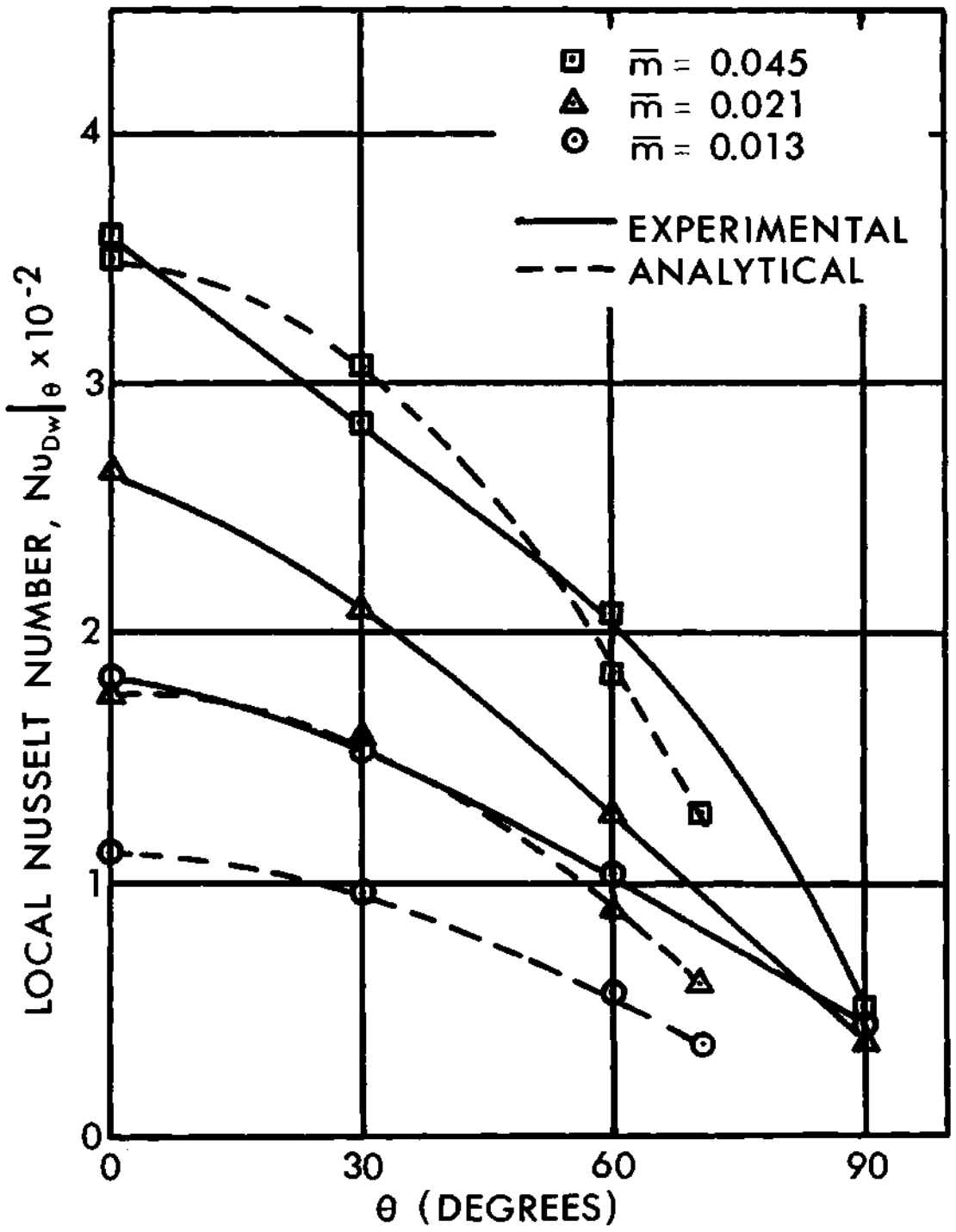

Figure 28. Comparison of Experimental and Analytical Local Nusselt Numbers for Re = 75,000 in Two-Component Flow.

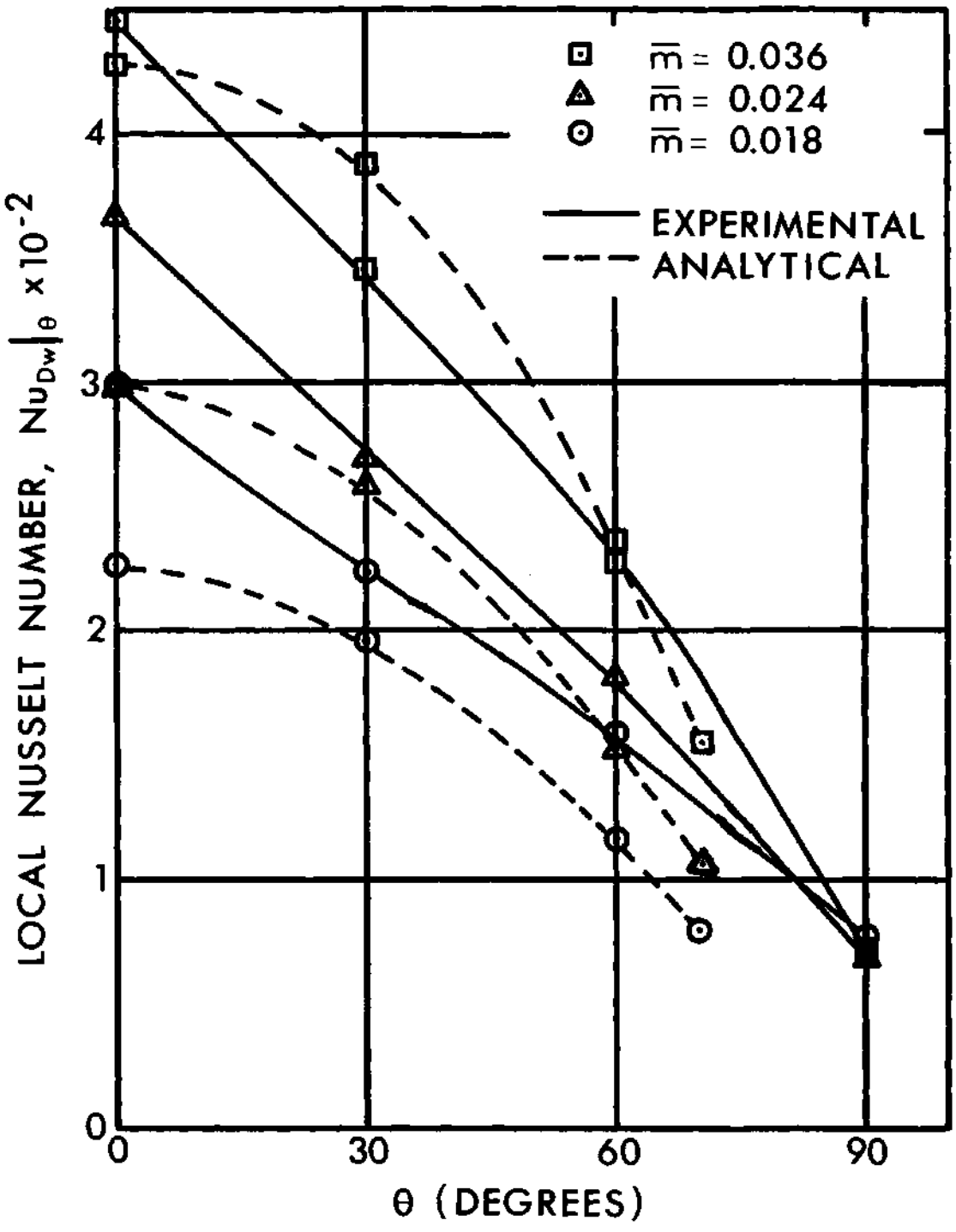

Figure 29. Comparison of Experimental and Analytical Local Nusselt Numbers for Re = 118,000 in Two-Component Flow.

numbers on the upstream side of a cylinder exposed to two-component (gas-liquid) crossflow. It was assumed that the gas boundary layer had no effect on the liquid boundary layer. Linear velocity and temperature profiles were assumed to exist in the liquid boundary layer. All the heat dissipated by the cylinder was assumed absorbed by the liquid film as sensible heat. Also, evaporation and convective heat transfer of the liquid film to the gas stream were considered negligible.

The film thickness (see page 46) was a function of the liquid Reynolds number and the angular position from the stagnation point and was independent of the liquid mass flow rate. The film thickness decreased with an increase in liquid Reynolds number and increased with the angular position from the stagnation point.

The film surface velocity increased from zero at the stagnation point to a maximum value of about 54 degrees from the stagnation point and then decreased again. The liquid film velocity increased with an increase in either the liquid Reynolds number or the liquid mass flow rate.

The local Nusselt number on the upstream side of the cylinder (see page 51) increased with an increase in either the liquid-gas mass flow rate ratio or the gas Reynolds number. Also, the local Nusselt number was a function of the liquid Prandtl number and the liquid-gas density and kinematic viscosity ratios. The local Nusselt number was a maximum at the stagnation point and decreased with an increase in angular position from the stagnation point.

Although the exact method of heat transfer from the cylinder was not determined, the analytical results did agree favorably with the experimental results when only sensible heating of the liquid film was con-

sidered. At the air Reynolds number of 30,000 (Figure 27), the analytical results agreed within ± 12 per cent of the experimental results. At the air Reynolds number of 75,000 (Figure 28), the analytical results were 20 to 40 per cent below the experimental results for the water-air mass flow rate ratios of 0.013 and 0.021. At the water-air mass flow rate ratio of 0.045, the analytical results were within ± 12 per cent of the experimental results. The poorest water spray droplet distribution was experienced at the air Reynolds number of 75,000. At the air Reynolds number of 118,000 (Figure 29), the analytical results were below, but within 30 per cent of the experimental results for the water-air mass flow rate ratios of 0.018 and 0.024. At the water-air mass flow rate ratios of 0.036, the analytical and experimental results were within ± 10 per cent of each other.

In comparing the experimental and analytical results it was apparent that the water-air mass flow rate ratio was a very critical factor and had to be determined accurately. Since a uniform spray was never obtained, the average water mass flow rate was rather arbitrary. This could have been a reason the experimental and analytical results did not consistently agree.

Closure

The results obtained from this investigation provide additional data on the heat transfer from an isothermal cylinder exposed to two-component (air-water) crossflow. The results seem to agree with the investigation of Smith (4), but seem to disagree to some extent with the investigation of Takahara (3). Considering the limited investigation in

this area and some conflict of data in these investigations, additional study is necessary to determine the important variables affecting the heat transfer characteristics and to resolve the disagreement in the present data.

CHAPTER VI

CONCLUSIONS AND RECOMMENDATIONS

The results obtained from this investigation of the heat transfer characteristics of an isothermal cylinder exposed to two-component (air-water) crossflow lead to the following conclusions:

1. The addition of water droplets to the air stream greatly increased the heat transfer from the cylinder.

2. The local Nusselt numbers on the upstream side of the cylinder increased with an increase in water-air mass flow rate ratio for a given Reynolds number.

3. The local Nusselt numbers on the downstream side of the cylinder remained fairly constant with an increase in water-air mass flow rate ratio for a given Reynolds number.

4. The maximum local Nusselt numbers were obtained at the cylinder stagnation point.

5. The overall Nusselt numbers for the cylinder increased with an increase in Reynolds number for a constant water-air mass flow rate ratio.

6. The overall Nusselt numbers for the cylinder increased with an increase in water-air mass flow rate ratio for a given Reynolds number.

7. A continuous liquid film covered the horizontally mounted test cylinder for all the tests.

8. The Nusselt numbers obtained from the simplified analytical model presented in this study compared favorably with the experimental

results, especially at the Reynolds number of 30,000.

The following items are recommended as a logical extension of this investigation:

1. Additional data should be obtained for a wider range of air free stream Reynolds numbers.

2. Tests at higher water-air mass flow rate ratios should be conducted to determine the upper limit of heat transfer from a cylinder exposed to two-component (air-water) crossflow.

3. Additional studies should be undertaken to determine the effects of droplet size and velocity on the heat transfer.

4. More studies should be conducted to develop nozzles which can deliver a uniform spray into the moving air stream.

5. Studies are needed to determine a reliable and easy method to obtain the average spray droplet velocity in the two-component flow.

6. Studies should be made to determine the heat transfer characteristics from the cylinder when liquid film evaporation is a significant factor.

7. A more detailed analytical study of the heat transfer characteristics of the liquid film on the upstream side of the cylinder is needed.

APPENDIX A

DETERMINATION OF WATER-AIR MASS FLOW RATE RATIO

To obtain the water-air mass flow rate ratio, it was necessary to first determine the water mass flow rate in the air stream and the air mass flow rate.

The equation used to determine the water mass flow rate from first obtaining the average water droplet collection rate was

$$\dot{m}_w = \left(\frac{4}{\pi d^2}\right)\left(N\right)\left(\rho_w\right)\left(3.53 \times 10^{-5}\right)$$

where

$\dot{m}_w$ = water mass flow rate (lbm/ft^2-sec)

$\frac{\pi d^2}{4}$ = area of collection probe (ft^2)

ρ_w = density of water (lbm/ft^3)

N = average water droplet collection rate (cc/sec)

The air mass flow rate was computed by using the continuity equation. The equation used was

$$\dot{m}_a = 2.66 \sqrt{\frac{\rho_{man}\, h}{T_\infty}\left[\frac{1 + \frac{\omega}{7000}}{1 + \frac{\omega}{4360}}\right]\left[P_{bar} + \frac{\Delta P}{13.6}\right]}$$

where

$\dot{m}_a$ = air mass flow rate (lbm/ft^2-sec)

ρ_{man} = density of micromanometer fluid (lbm/ft^3)

h = micromanometer reading of velocity pressure ("H_2O)

ω = absolute humidity of air (gr/lbmda)

T_∞ = temperature of air (^oR)

P_{bar} = barometric pressure at 32^oF ("Hg)

ΔP = static pressure at test section area ("H_2O)

The procedure used for collecting the data needed for these two equations was described in detail in Chapter III.

From these two equations, the water-air mass flow rate ratio was

$$\bar{m} = \frac{\dot{m}_w}{\dot{m}_a} \quad .$$

APPENDIX B

TABULAR DATA FOR HEAT TRANSFER TESTS

The heat transfer tests were made in two separate series of runs. In the first series, heater #3 was the stagnation point heater and only one SQ-10 nozzle was used to produce the water spray droplets. During these tests, the wattage output of heater #2 (30 degrees from the stagnation point) was equal to or greater than the wattage output of the stagnation point heater (heater #3). In the second series of runs, the cylinder was rotated 30 degrees so heater #4 became the stagnation point heater. This rotation alleviated the problem of high wattage output experienced at 30 degrees from the stagnation point and resulted in fairly symmetric wattage loads. For higher water mass flow rates, a second SQ-10 nozzle was installed.

The following tests were made in the first series of runs and are listed in chronological order:

A-50-1

A-20-1

A-80-1

AW-50-2

AW-50-1

AW-20-3

AW-20-2

AW-20-1

AW-80-1

AW-80-3

AW-80-2

The following tests were made in the second series of runs and are listed in chronological order:

AW-20-4

AW-50-7

AW-50-5

AW-50-3

AW-50-4

AW-80-4

AW-80-5

AW-20-6

AW-20-5

AW-50-6

AW-80-6

The notation used to identify the test runs was as follows:

A denoted air flow,

AW denoted air-water flow,

20, 50, and 80 denoted the air velocity (ft/sec), and

1, 2, 3, etc. denoted the test number at certain flow conditions.

The results of heat transfer from the cylinder exposed to one-component (air) flow are presented in Tables 1 through 4. The results of heat transfer in two-component (air-water) flow are presented in Tables 1 and 5 through 22. The dependency of the temperature difference between the cylinder surface and the free stream reference temperature on the

heat transfer is presented in Table 23.

The Nusselt numbers for the one-component (air) flow were based on the air thermal conductivity and the cylinder diameter. In Figures 21, 22, 23, and 26, the overall Nusselt numbers for zero water-air mass flow rate ratio (air flow) were based on the water thermal conductivity. The Nusselt numbers for the two-component (air-water) flow were based on the water thermal conductivity and the cylinder diameter.

Table 1. Summary of Experimental Heat Transfer Data

Test No.	Reynolds Number	Water-Air Mass Flow Rate Ratio	Overall Nusselt Number
A-20-1	30,000	0.000	145
AW-20-1	30,000	0.028	58
AW-20-2	30,000	0.038	63
AW-20-3	30,000	0.057	82
AW-20-4	30,000	0.079	102
AW-20-5	30,000	0.097	115
AW-20-6	30,000	0.130	145
A-50-1	75,000	0.000	240
AW-50-1	75,000	0.013	88
AW-50-2	75,000	0.021	121
AW-50-3	75,000	0.024	127
AW-50-4	75,000	0.031	156
AW-50-5	75,000	0.045	165
AW-50-6	75,000	0.061	175
A-80-1	118,000	0.000	391
AW-80-1	118,000	0.012	124
AW-80-2	118,000	0.018	147
AW-80-3	118,000	0.024	173
AW-80-4	118,000	0.029	188
AW-80-5	118,000	0.036	198
AW-80-6	118,000	0.044	226

Table 2. Heat Transfer in One-Component (Air) Flow

Test No. A-20-1

Reynolds Number: 30,000

Air Dry Bulb Temperature (T_∞): 71.0°F

Relative Humidity: 97%

θ degrees	T_s °F	$T_s - T_\infty$ °F	Heat Flux BTU/hr.ft.^{2}	$Nu_{Da\|\theta}$ Local Nusselt Number
0	124.5	53.5	516	157
30	124.4	53.3	352	108
60	124.0	53.0	430	132
90	124.4	53.4	281	85
120	124.4	53.4	156	47
150	124.0	53.0	742	228
180	124.3	53.3	828	252
210	124.2	53.2	735	224
240	124.4	53.4	296	90
270	124.3	53.3	195	59
300	124.8	53.8	375	113
330	123.7	52.7	600	185

Table 3. Heat Transfer in One-Component (Air) Flow

Test No. A-50-1

Reynolds Number: 75,000

Air Dry Bulb Temperature (T_∞): 74.3°F

Relative Humidity: 98%

θ degrees	T_s °F	$T_s - T_\infty$ °F	Heat Flux BTU/hr.ft.^{2}	$Nu_{Da\|\theta}$ Local Nusselt Number
0	115.7	41.4	655	256
30	115.7	41.4	469	183
60	115.3	41.0	430	170
90	115.9	41.6	469	183
120	115.9	41.6	274	107
150	115.4	41.1	968	382
180	115.8	41.5	1,015	396
210	115.4	41.1	945	374
240	115.4	41.1	382	151
270	115.5	41.2	312	122
300	116.0	41.7	516	200
330	114.8	40.5	664	266

Table 4. Heat Transfer in One-Component (Air) Flow

Test No. A-80-1

Reynolds Number: 118,000

Air Dry Bulb Temperature (T_∞): 76.9°F

Relative Humidity: 96%

θ degrees	T_s °F	$T_s - T_\infty$ °F	Heat Flux BTU/hr.ft.^{2}	$Nu_{Da\|\theta}$ Local Nusselt Number
0	117.1	40.2	1,210	489
30	116.9	40.0	734	297
60	117.1	40.2	734	296
90	117.5	40.6	780	312
120	117.3	40.4	718	289
150	116.9	40.0	1,258	510
180	117.3	40.4	1,367	548
210	116.7	39.8	1,220	497
240	116.5	39.6	750	307
270	116.5	39.6	648	263
300	117.5	40.6	804	322
330	115.3	38.4	1,093	461

Table 5. Heat Transfer in Two-Component (Air-Water) Flow

Test No. AW-20-1

Reynolds Number: 30,000

Water-Air Mass Flow Rate Ratio: 0.028

Average Water Mass Flow Rate: 0.0395 lbm/ft^2-sec
Spray Droplet Distribution Variation: ± 24%
Approximate Median Water Droplet Diameter: 230 microns
Nozzle: 1 SQ-10
Operating Pressure: 60 psig

Spray Water Temperature (T_∞): 78.0°F
Air Dry Bulb Temperature: 78.0°F
Relative Humidity: 93%

θ degrees	T_s °F	$T_s - T_\infty$ °F	Heat Flux BTU/hr.ft.^{2}	$Nu_{Dw\|\theta}$ Local Nusselt Number
0	111.3	33.3	5,035	108
30	110.8	32.8	4,440	96
330	111.3	33.3	5,840	121
60	111.0	33.0	3,080	66
300	111.7	33.7	2,970	61
90	111.3	33.3	1,125	24
270	110.6	32.6	1,140	24
120	111.3	33.3	1,030	22
240	111.5	33.5	1,205	25
150	111.0	33.0	2,050	44
210	111.5	33.5	1,920	40
180	111.5	33.5	2,050	43

Table 6. Heat Transfer in Two-Component (Air-Water) Flow

Test No. AW-20-2

Reynolds Number: 30,000

Water-Air Mass Flow Rate Ratio: 0.038

Average Water Mass Flow Rate: 0.0544 lbm/ft^2-sec
Spray Droplet Distribution Variation: ± 23%
Approximate Median Water Droplet Diameter: 175 microns
Nozzle: 1 SQ-10
Operating Pressure: 100 psig

Spray Water Temperature (T_∞): 79.2°F
Air Dry Bulb Temperature: 79.0°F
Relative Humidity: 99%

θ degrees	T_s °F	$T_s - T_\infty$ °F	Heat Flux BTU/hr.ft.^{2}	$Nu_{Dw\|\theta}$ Local Nusselt Number
0	109.5	30.3	5,330	126
30	109.2	30.0	4,440	105
330	109.3	30.1	5,775	132
60	108.9	29.7	2,870	69
300	110.1	30.9	3,295	74
90	109.3	30.1	1,280	31
270	108.2	29.0	765	17
120	109.1	29.9	1,065	25
240	109.1	29.9	922	21
150	108.7	29.5	1,845	44
210	109.3	30.1	1,295	30
180	109.1	29.9	1,765	42

Table 7. Heat Transfer in Two-Component (Air-Water) Flow

Test No. AW-20-3

Reynolds Number: 30,000

Water-Air Mass Flow Rate Ratio: 0.057

Average Water Mass Flow Rate: 0.0805 lbm/ft^2-sec
Spray Droplet Distribution Variation: ± 12%
Approximate Median Water Droplet Diameter: 120 microns
Nozzle: 1 SQ-10
Operating Pressure: 200 psig

Spray Water Temperature (T_∞): 79.5°F
Air Dry Bulb Temperature: 78.0°F
Relative Humidity: 93%

θ degrees	T_s °F	$T_s - T_\infty$ °F	Heat Flux BTU/hr.ft.^{2}	$Nu_{Dw\|\theta}$ Local Nusselt Number
0	110.2	30.7	7,730	180
30	110.2	30.7	6,090	141
330	109.8	30.3	7,770	177
60	110.1	30.6	3,740	87
300	110.4	30.9	4,075	91
90	110.3	30.8	1,530	36
270	109.0	29.5	1,060	24
120	110.0	30.5	1,220	28
240	110.2	30.7	1,000	23
150	110.2	30.7	2,455	57
210	110.2	30.7	1,080	24
180	110.6	31.1	1,890	43

Table 8. Heat Transfer in Two-Component (Air-Water) Flow

Test No. AW-20-4

Reynolds Number: 30,000

Water-Air Mass Flow Rate Ratio: 0.079

Average Water Mass Flow Rate: 0.112 lbm/ft^2-sec
Spray Droplet Distribution Variation: ± 28%
Approximate Median Water Droplet Diameter: 175 microns
Nozzle: 2 SQ-10
Operating Pressure: 100 psig

Spray Water Temperature (T_∞): 79.7°F
Air Dry Bulb Temperature: 78.5°F
Relative Humidity: 92%

θ degrees	T_s °F	$T_s - T_\infty$ °F	Heat Flux BTU/hr.ft.^{2}	$Nu_{Dw\|\theta}$ Local Nusselt Number
0	110.8	31.1	9,600	219
30	110.4	30.7	7,430	167
330	110.6	30.9	8,000	183
60	110.6	30.9	5,620	130
300	110.4	30.7	5,940	133
90	110.8	31.1	1,092	25
270	110.8	31.1	750	17
120	110.4	30.7	3,123	73
240	110.2	30.5	2,880	65
150	110.8	31.1	1,592	36
210	110.4	30.7	875	19
180	110.4	30.7	2,185	51

Table 9. Heat Transfer in Two-Component (Air-Water) Flow

Test No. AW-20-5

Reynolds Number: 30,000

Water-Air Mass Flow Rate Ratio: 0.097

Average Water Mass Flow Rate: 0.136 lbm/ft^2-sec
Spray Droplet Distribution Variation: ± 33%
Approximate Median Water Droplet Diameter: 185 microns
Nozzle: 2 SQ-10
Operating Pressure: 90 psig

Spray Water Temperature (T_∞): 81.1°F
Air Dry Bulb Temperature: 80.5°F
Relative Humidity: 96%

θ degrees	T_s °F	$T_s - T_\infty$ °F	Heat Flux BTU/hr.ft.^{2}	$Nu_{Dw\|\theta}$ Local Nusselt Number
0	113.2	32.1	12,200	271
30	113.2	32.1	8,050	173
330	112.9	31.8	9,530	214
60	113.4	32.3	7,380	157
300	113.2	32.1	6,440	142
90	112.9	31.8	935	20
270	113.9	32.8	2,340	51
120	112.9	31.8	2,660	57
240	112.9	31.8	2,340	52
150	113.4	32.3	2,120	46
210	113.5	32.4	1,562	34
180	113.4	32.3	1,970	43

Table 10. Heat Transfer in Two-Component (Air-Water) Flow

Test No. AW-20-6

Reynolds Number: 30,000

Water-Air Mass Flow Rate Ratio: 0.130

Average Water Mass Flow Rate: 0.180 lbm/ft^2-sec
Spray Droplet Distribution Variation: ± 13%
Approximate Median Water Droplet Diameter: 145 microns
Nozzle: 2 SQ-10
Operating Pressure: 140 psig

Spray Water Temperature (T_∞): 79.5°F
Air Dry Bulb Temperature: 79.0°F
Relative Humidity: 92%

θ degrees	T_s °F	$T_s - T_\infty$ °F	Heat Flux BTU/hr.ft.^{2}	$Nu_{Dw\|\theta}$ Local Nusselt Number
0	109.9	30.4	16,500	402
30	109.4	29.9	11,120	264
330	109.9	30.4	12,100	284
60	109.7	30.2	8,280	195
300	109.5	30.0	6,630	157
90	110.2	30.7	2,030	49
270	110.0	30.5	2,500	58
120	110.2	30.7	2,660	62
240	109.1	29.6	1,780	43
150	110.1	30.6	1,780	43
210	109.5	30.0	1,340	32
180	109.8	30.3	1,590	37

Table 11. Heat Transfer in Two-Component (Air-Water) Flow

Test No. AW-50-1

Reynolds Number: 75,000

Water-Air Mass Flow Rate Ratio: 0.013

Average Water Mass Flow Rate: 0.045 lbm/ft^2-sec
Spray Droplet Distribution Variation: ± 23%
Approximate Median Water Droplet Diameter: 255 microns
Nozzle: 1 SQ-10
Operating Pressure: 50 psig

Spray Water Temperature (T_∞): 82.5°F
Air Dry Bulb Temperature: 82.0°F
Relative Humidity: 96%

θ degrees	T_s °F	$T_s - T_\infty$ °F	Heat Flux BTU/hr.ft.^{2}	$Nu_{Dw\|\theta}$ Local Nusselt Number
0	112.9	30.4	7,930	185
30	112.9	30.4	6,560	153
330	113.1	30.6	8,780	204
60	112.4	29.9	4,375	104
300	113.3	30.8	4,840	112
90	112.5	30.0	1,780	42
270	112.3	30.5	1,530	36
120	113.2	30.7	1,405	33
240	112.7	30.2	1,720	41
150	112.5	30.0	3,280	78
210	112.3	29.8	1,590	38
180	113.1	30.6	2,685	63

Table 12. Heat Transfer in Two-Component (Air-Water) Flow

Test No. AW-50-2

Reynolds Number: 75,000

Water-Air Mass Flow Rate Ratio: 0.021

Average Water Mass Flow Rate: 0.075 lbm/ft^2-sec
Spray Droplet Distribution Variation: ± 33%
Approximate Median Water Droplet Diameter: 175 microns
Nozzle: 1 SQ-10
Operating Pressure: 100 psig

Spray Water Temperature (T_∞): 82.5°F
Air Dry Bulb Temperature: 80.0°F
Relative Humidity: 96%

θ degrees	T_s °F	$T_s - T_\infty$ °F	Heat Flux BTU/hr.ft.^{2}	$Nu_{Dw\|\theta}$ Local Nusselt Number
0	111.5	29.0	10,780	264
30	111.7	29.2	8,620	210
330	111.4	28.9	11,550	285
60	111.7	29.2	5,210	127
300	112.0	29.5	5,880	142
90	112.0	29.5	2,340	56
270	110.9	28.4	1,562	39
120	112.1	29.6	718	17
240	111.8	29.3	1,470	36
150	112.3	29.8	3,440	82
210	111.5	29.0	2,060	51
180	111.8	29.3	4,410	107

Table 13. Heat Transfer in Two-Component (Air-Water) Flow

Test No. AW-50-3

Reynolds Number: 75,000

Water-Air Mass Flow Rate Ratio: 0.024

Average Water Mass Flow Rate: 0.085 lbm/ft^2-sec
Spray Droplet Distribution Variation: ± 26%
Approximate Median Water Droplet Diameter: 335 microns
Nozzle: 2 SQ-10
Operating Pressure: 30 psig

Spray Water Temperature (T_∞): 82.5°F
Air Dry Bulb Temperature: 80.0°F
Relative Humidity: 90%

θ degrees	T_s °F	$T_s - T_\infty$ °F	Heat Flux BTU/hr.ft.^{2}	$Nu_{Dw\|\theta}$ Local Nusselt Number
0	112.1	29.6	11,400	274
30	111.8	29.3	7,720	187
330	112.5	30.0	9,490	225
60	111.7	29.2	6,590	160
300	112.1	29.6	6,490	156
90	112.5	30.0	2,380	56
270	112.4	29.9	1,875	45
120	111.8	29.3	2,660	64
240	111.5	29.0	2,060	51
150	112.3	29.8	2,970	70
210	112.1	29.6	2,660	64
180	112.1	29.6	3,060	73

Table 14. Heat Transfer in Two-Component (Air-Water) Flow

Test No. AW-50-4

Reynolds Number: 75,000

Water-Air Mass Flow Rate Ratio: 0.031

Average Water Mass Flow Rate: 0.110 lbm/ft^2-sec
Spray Droplet Distribution Variation: ± 40%
Approximate Median Water Droplet Diameter: 255 microns
Nozzle: 2 SQ-10
Operating Pressure: 50 psig

Spray Water Temperature (T_∞): 82.0°F
Air Dry Bulb Temperature: 81.2°F
Relative Humidity: 92%

θ degrees	T_s °F	$T_s - T_\infty$ °F	Heat Flux BTU/hr.ft.^{2}	$Nu_{Dw\|\theta}$ Local Nusselt Number
0	111.7	29.7	14,050	337
30	111.7	29.7	9,970	237
330	111.9	29.9	11,050	263
60	111.9	29.9	8,900	211
300	112.1	30.1	8,120	192
90	112.1	30.1	2,100	49
270	112.1	30.1	1,910	45
120	111.5	29.5	3,380	81
240	112.1	30.1	3,620	85
150	112.1	30.1	3,620	85
210	112.1	30.1	2,625	62
180	112.1	30.1	3,530	83

Table 15. Heat Transfer in Two-Component (Air-Water) Flow

Test No. AW-50-5

Reynolds Number: 75,000

Water-Air Mass Flow Rate Ratio: 0.045

Average Water Mass Flow Rate: 0.158 lbm/ft^2-sec
Spray Droplet Distribution Variation: ± 45%
Approximate Median Water Droplet Diameter: 210 microns
Nozzle: 2 SQ-10
Operating Pressure: 70 psig

Spray Water Temperature (T_∞): 81.0°F
Air Dry Bulb Temperature: 80.5°F
Relative Humidity: 92%

θ degrees	T_s °F	$T_s - T_\infty$ °F	Heat Flux BTU/hr.ft.^{2}	$Nu_{Dw}\|\theta$ Local Nusselt Number
0	110.0	29.0	14,680	360
30	109.5	28.5	9,680	241
330	109.5	28.5	11,400	284
60	109.5	28.5	9,060	226
300	110.0	29.0	8,440	206
90	110.5	29.5	3,230	78
270	110.5	29.5	2,110	51
120	109.5	28.5	3,400	85
240	109.0	28.0	3,220	83
150	110.0	29.0	3,440	84
210	110.5	29.5	3,440	83
180	110.0	29.0	3,590	88

Table 16. Heat Transfer in Two-Component (Air-Water) Flow

Test No. AW-50-6

Reynolds Number: 75,000

Water-Air Mass Flow Rate Ratio: 0.061

Average Water Mass Flow Rate: 0.213 lbm/ft^2-sec
Spray Droplet Distribution Variation: ± 45%
Approximate Median Water Droplet Diameter: 175 microns
Nozzle: 2 SQ-10
Operating Pressure: 100 psig

Spray Water Temperature (T_∞): 81.2°F
Air Dry Bulb Temperature: 81.8°F
Relative Humidity: 95%

θ degrees	T_s °F	$T_s - T_\infty$ °F	Heat Flux BTU/hr.ft.^{2}	$Nu_{Dw\|\theta}$ Local Nusselt Number
0	110.6	29.4	15,870	381
30	111.0	29.8	12,940	309
330	110.6	29.4	7,970	193
60	110.8	29.6	9,540	229
300	109.9	28.7	9,220	228
90	111.4	30.2	2,500	59
270	110.6	29.4	2,530	61
120	110.4	29.2	3,440	84
240	110.4	29.2	2,880	70
150	110.8	29.6	3,310	80
210	109.9	28.7	2,190	54
180	110.2	29.0	3,500	86

Table 17. Heat Transfer in Two-Component (Air-Water) Flow

Test No. AW-80-1

Reynolds Number: 118,000

Water-Air Mass Flow Rate Ratio: 0.012

Average Water Mass Flow Rate: 0.070 lbm/ft^2-sec
Spray Droplet Distribution Variation: ± 45%
Approximate Median Water Droplet Diameter: 175 microns
Nozzle: 1 SQ-10
Operating Pressure: 100 psig

Spray Water Temperature (T_∞): 79.2°F
Air Dry Bulb Temperature: 78.0°F
Relative Humidity: 90%

θ degrees	T_s °F	$T_s - T_\infty$ °F	Heat Flux BTU/hr.ft.^{2}	$Nu_{Dw\|\theta}$ Local Nusselt Number
0	108.9	29.7	10,180	244
30	108.0	28.8	7,810	193
330	108.9	29.7	10,100	242
60	108.0	28.8	5,310	131
300	109.1	29.9	6,120	145
90	109.0	29.8	3,320	79
270	109.0	29.8	2,780	66
120	108.3	29.1	2,340	59
240	109.8	30.6	2,810	66
150	109.1	29.9	3,590	85
210	109.0	29.8	2,960	71
180	109.4	30.4	4,060	95

Table 18. Heat Transfer in Two-Component (Air-Water) Flow

Test No. AW-80-2

Reynolds Number: 118,000

Water-Air Mass Flow Rate Ratio: 0.018

Average Water Mass Flow Rate: 0.100 lbm/ft^2-sec
Spray Droplet Distribution Variation: ± 24%
Approximate Median Water Droplet Diameter: 140 microns
Nozzle: 1 SQ-10
Operating Pressure: 150 psig

Spray Water Temperature (T_∞): 77.5°F
Air Dry Bulb Temperature: 76.8°F
Relative Humidity: 97%

θ degrees	T_s °F	$T_s - T_\infty$ °F	Heat Flux BTU/hr.ft.^{2}	$Nu_{Dw\|\theta}$ Local Nusselt Number
0	108.0	30.5	12,810	299
30	107.0	29.5	9,250	223
330	107.3	29.8	12,650	302
60	107.7	30.2	6,780	160
300	108.2	30.7	7,210	167
90	108.1	30.6	3,370	78
270	106.6	29.1	2,810	68
120	108.1	30.6	2,940	68
240	107.3	29.8	3,310	79
150	107.3	29.8	4,650	111
210	108.0	30.5	3,530	83
180	107.6	30.1	4,970	117

Table 19. Heat Transfer in Two-Component (Air-Water) Flow

Test No. AW-80-3

Reynolds Number: 118,000

Water-Air Mass Flow Rate Ratio: 0.024

Average Water Mass Flow Rate: 0.135 lbm/ft^2-sec
Spray Droplet Distribution Variation: ± 30%
Approximate Median Water Droplet Diameter: 115 microns
Nozzle: 1 SQ-10
Operating Pressure: 224 psig

Spray Water Temperature (T_∞): 77.3°F
Air Dry Bulb Temperature: 77.0°F
Relative Humidity: 95%

θ degrees	T_s °F	$T_s - T_\infty$ °F	Heat Flux BTU/hr.ft.^{2}	$Nu_{Dw\|\theta}$ Local Nusselt Number
0	107.6	30.3	15,620	366
30	107.6	30.3	11,470	269
330	107.2	29.9	15,480	372
60	107.3	30.0	6,660	158
300	108.3	31.0	7,940	182
90	107.3	30.0	3,000	71
270	105.4	28.1	1,750	44
120	107.3	30.0	3,120	74
240	107.1	29.8	3,720	89
150	107.2	29.9	4,840	115
210	107.3	30.0	3,530	84
180	107.3	30.0	5,590	132

Table 20. Heat Transfer in Two-Component (Air-Water) Flow

Test No. AW-80-4

Reynolds Number: 118,000

Water-Air Mass Flow Rate Ratio: 0.029

Average Water Mass Flow Rate: 0.162 lbm/ft^2-sec
Spray Droplet Distribution Variation: ± 25%
Approximate Median Water Droplet Diameter: 210 microns
Nozzle: 2 SQ-10
Operating Pressure: 70 psig

Spray Water Temperature (T_∞): 80.8°F
Air Dry Bulb Temperature: 80.5°F
Relative Humidity: 95%

θ degrees	T_s °F	$T_s - T_\infty$ °F	Heat Flux BTU/hr.ft.^{2}	$Nu_{Dw\|\theta}$ Local Nusselt Number
0	110.8	30.0	17,050	406
30	110.8	30.0	12,250	291
330	110.8	30.0	14,120	335
60	110.6	29.8	10,550	252
300	110.8	30.0	9,900	235
90	111.0	30.2	2,530	60
270	111.0	30.2	2,720	64
120	110.6	29.8	3,940	94
240	110.4	29.6	3,690	88
150	111.2	30.4	3,680	86
210	110.8	30.0	2,660	64
180	110.8	30.0	4,340	103

Table 21. Heat Transfer in Two-Component (Air-Water) Flow

Test No. AW-80-5

Reynolds Number: 118,000

Water-Air Flow Rate Ratio: 0.036

Average Water Mass Flow Rate: 0.206 lbm/ft^2-sec
Spray Droplet Distribution Variation: ± 28%
Approximate Median Water Droplet Diameter: 160 microns
Nozzle: 2 SQ-10
Operating Pressure: 120 psig

Spray Water Temperature (T_∞): 79.1°F
Air Dry Bulb Temperature: 79.7°F
Relative Humidity: 96%

θ degrees	T_s °F	$T_s - T_\infty$ °F	Heat Flux BTU/hr.ft.^{2}	$Nu_{Dw\|\theta}$ Local Nusselt Number
0	109.6	30.6	19,250	448
30	109.6	30.6	13,550	315
330	110.2	31.1	15,100	346
60	110.0	30.9	11,800	271
300	109.5	30.4	10,000	234
90	110.4	31.3	2,750	63
270	110.4	31.3	3,060	70
120	109.6	30.5	4,500	100
240	109.9	30.8	4,120	95
150	110.6	31.5	4,370	88
210	110.0	30.9	2,870	66
180	109.6	30.6	3,590	102

Table 22. Heat Transfer in Two-Component (Air-Water) Flow

Test No. AW-80-6

Reynolds Number: 118,000

Water-Air Mass Flow Rate Ratio: 0.044

Average Water Mass Flow Rate: 0.249 lbm/ft^2-sec
Spray Droplet Distribution Variation: ± 17%
Approximate Median Water Droplet Diameter: 145 microns
Nozzle: 2 SQ-10
Operating Pressure: 140 psig

Spray Water Temperature (T_∞): 79.7°F
Air Dry Bulb Temperature: 80.3°F
Relative Humidity: 90%

θ degrees	T_s °F	$T_s - T_\infty$ °F	Heat Flux BTU/hr.ft.^{2}	$Nu_{Dw\|\theta}$ Local Nusselt Number
0	108.8	29.1	22,800	557
30	108.5	28.8	14,980	370
330	108.7	29.0	15,620	384
60	108.4	28.7	12,520	310
300	108.5	28.8	10,550	260
90	108.7	29.0	2,500	61
270	108.5	28.8	1,875	46
120	108.7	29.0	4,090	100
240	108.7	29.0	4,720	106
150	109.1	29.4	3,650	88
210	109.4	29.7	3,500	84
180	109.1	29.4	4,220	102

Table 23. Heat Transfer in Two-Component (Air-Water) Flow

Test No. AW-50-7

Reynolds Number: 75,000

Water-Air Mass Flow Rate Ratio: 0.058

Spray Water Temperature (T_∞): 79.3°F, 80.1°F, 81.0°F

Air Dry Bulb Temperature: 80.5°F

Relative Humidity: 90%

Average Water Mass Flow Rate: 0.206 lbm/ft^2-sec

Spray Droplet Distribution Variation: ± 41%

Approximate Median Water Droplet Diameter: 175 Microns

Nozzle: 2 SQ-10

Operating Pressure: 100 psig

θ degrees	$T_s - T_\infty$ °F Runs			Heat Flux BTU/hr.ft.^{2} Runs			$Nu_{Dw}\|_\theta$ Local Nusselt Number Runs		
	A	B	C	A	B	C	A	B	C
0	20.8	31.8	43	9,120	14,250	20,300	312	318	340
30	20.7	32.0	43	6,275	9,470	14,850	216	228	245
330	21.5	32.0	43	8,070	12,050	17,000	266	268	280
60	20.8	32.4	43	5,030	8,720	12,300	180	185	203
300	20.8	31.8	43	5,150	8,470	12,450	177	188	206
90	21.1	32.9	43	1,435	2,160	2,830	48	47	47
270	21.1	32.0	43	1,220	1,655	2,060	41	37	34
120	20.4	32.0	43	1,940	3,440	4,375	68	76	73
240	20.0	31.6	43	2,250	4,400	5,000	80	99	83
150	20.7	32.9	43	1,940	3,910	5,470	66	85	90
210	20.7	32.0	43	1,910	3,060	3,750	66	68	62
180	20.9	31.6	43	1,910	3,750	7,810	65	85	129

LITERATURE CITED

1. A. Acrivos, J. E. Ahern, and A. R. Nagy, Jr., Research Investigation of Two-Component Heat Transfer, The Marquardt Corporation, ARL Report ARL 64-116, Wright-Patterson AFB, Ohio, June, 1964.

2. F. Hoelscher, Study of Heat Transfer from a Heated Cylinder in Two-Phase, Water-Air Flow, Master's Thesis, Air Force Institute of Technology, Wright-Patterson AFB, Ohio, March, 1965.

3. E. W. Takahara, Experimental Study of Heat Transfer from a Heated Circular Cylinder in Two-Phase, Water-Air, Flow, Master's Thesis, Air Force Institute of Technology, Wright-Patterson AFB, Ohio, March, 1966.

4. J. E. Smith, Heat Transfer Studies of Water-Spray Flows, Northern Research and Engineering Corporation, ARL Report ARL 66-0091, Wright-Patterson AFB, Ohio, May, 1966.

5. A. N. Tifford, Exploratory Investigation of Laminar Boundary Layer Heat Transfer Characteristics of Gas-Liquid-Spray Systems, Ohio State University Research Foundation, ARL Report ARL 64-136, Wright-Patterson AFB, Ohio, September, 1964.

6. M. E. Goldstein, Wen-Jei Yang, and J. A. Clark, Boundary Layer Analysis of Two-Phase Flow Over a Circular Cylinder and Oscillating Flat Plate, Heat Transfer Laboratory Technical Report No. 5, University of Michigan, Under Contract with Aerospace Research Laboratories, September, 1965.

7. E. A. Brun, Icing Problems and Recommended Solutions, North Atlantic Treaty Organization, Advisory Group for Aeronautical Research and Development, November, 1957, pp. 170-173.

8. J. L. Dussourd, A Theoretical and Experimental Investigation of a Deceleration Probe for Measurement of Several Properties of a Droplet-Laden Air Stream, Doctor of Science in Mechanical Engineering Thesis, M.I.T., Cambridge, Massachusetts, October, 1954.

9. J. Sucec, On the Correction of the Reading Recorded by an Impact Tube Inserted into a Gas Stream Containing Entrained Liquid Particles, Project Note NASA No. 9, Mechanical Engineering Department, University of Connecticut, Storrs, Connecticut, August, 1963.

10. A. Fage and V. M. Falkner, "Further Experiments on the Flow Around a Circular Cylinder," Great Britain Aeronautical Research Council R & M 1369, 1931.

11. R. Hilpert, "Wärmeabgabe von geheizten Drähten and Rohren," Forsch. Gebiete Ingenieurwesen, Volume 4, 1933, Abstract 9, p. 220.

12. W. H. McAdams, Heat Transmission, McGraw-Hill Book Company, Inc., New York, 1942, pp. 225-226.